Applied Biochemistry and Biotechnology
https://doi.org/10.1007/s12010-022-04277-w

ORIGINAL ARTICLE

Polyaniline Entrapped Water-Dispersible 3MPA-ZnSe Quantum Dots and Their Application for the Development of an Enzymatic Electrochemical Nanobiosensor for the Detection of 17β-Estradiol, an Endocrine-Disrupting Compound

Abongile Nwabisa Jijana[1,2]

Accepted: 16 December 2022

Abstract
17β-estradiol is used as a growth and fertility stimulant in the agronomic sector to induce fertility and manipulate reproductive characteristics in animals. However, unintended or unregulated distribution and exposure to even significant low levels of 17β-estradiol estrogen have detrimental health implication that can lead to reproductive abnormalities and even cancer. This could have severe effect on the ecosystem imbalance, food safety, to such a degree that its health impact necessitates rapid methods to probe for its prevalence and occurrence in the environment. Herein a simple, robust, sensitive and once-off use electrochemical biosensor to detect 17β-estradiol is developed, using 3-mercaptopropionic acid capped zinc selenide quantum dots trapped within the polyaniline (PANI) framework structure. The biosensor's interaction with the substrate was based on the capability of the hemeprotein, horseradish peroxidase (HRP) enzyme (i.e., baroreceptor) to alternatively catalyze phenolic alcohols. The biosensor displayed a significantly low limit of detection limit (LOD) of value 0.2×10^{-6} M towards 17β-estradiol. The Mechaelis-Menten constant (K_m) with the magnitude of 0.64×10^{-6} M was obtained; this indicates an outstanding affinity of the biosensing films towards 17β-estradiol. Subsequently, the developed biosensor was able to accurately and efficiently measure successive concentrations of 17β-estradiol from 0.2×10 to 4×10^{-6} M. The fabricated biosensor showed good selectivity towards 17β-estradiol compared to the other estrogenic endocrine-disrupting compounds such as estrone (E1), ethnylstradiol (EE2), and estriol (E3). The biosensor was capable of detecting 17β-estradiol in spiked tap water samples with good recoveries, thus affirming its potential to be applied for real electro-analysis of 17β-estradiol in treated wastewater.

Keywords Estrogenic endocrine-disrupting compounds (e-EDC) · 17β-estradiol (E2); hormone replacement therapy (HRT) · Quantum dots · Polymer nanocomposites · Polyaniline (PANI) · Electrochemical biosensors

✉ Abongile Nwabisa Jijana
abongilejijana@gmail.com; AbongileJ@mintek.co.za

Extended author information available on the last page of the article

Introduction

17β-estradiol is one of the most potent natural estrogen with crucial physiological properties, attributable to its significant role during development and growth of the reproductive cycle, nervous system, and for partial regulation of many metabolic pathways [2]. The same properties have prompted researchers in the branch of medicine to establish estrogen therapies, hence its fast-growing prescribed pharmaceutical use. 17β-estradiol is one the most potent estrogens amongst other estrogens, due to its significant prevalence in the environment and its toxicity. At even relatively low concentrations, 17β-estradiol can result in complete disruption and impairment of the endocrine system [1], whose function is to regulate the secretion and distribution of hormones in *homo sapiens* and other mammalian species [2]. The endocrine system consists of a series of glands that secrete natural hormones together with the associated receptors that respond to these hormones [3, 4]. Even though steroid hormones such as 17β-estradiol play a significant role in regulation and development of the reproductive system, estrogens possess major health risks to human life and other vertebrates, predominantly aquatic species [3, 5, 6].

Estrogens at relative accumulative concentrations are also classified as estrogenic endocrine-disrupting compounds. These are chemical or exogenous compounds that disrupt or interfere with the synthesis, secretion, binding, and action of natural hormones in the endocrine system [3, 7]. Estrogens frequently bind to relative receptor sites and enzymes, and have the ability to trigger spontaneous activity of the reproductive cycle, an occurrence observed in both males and females. Subsequently, these interactions can alter disproportionate estrogen activity and result in complete interruption of the estrogenic and reproductive cycle [8]. Potential estrogenic endocrine-disrupting compounds include natural steroids, synthetic hormones [9, 10] and other chemical compounds with significant structural similarities to natural estrogens. Estrogenic endocrine-disrupting compounds can be classified as natural female hormones (i.e., natural estrogens) and synthetic estrogens. Figure 1 illustrates the chemical structures of four well-known estrogenic endocrine disruptors; 17β-estradiol (E2) estrone (E1), estriol (E3), and 17α-ethnylestradiol (EE2). Ethnylestradiol-17α (EE2) is a synthetic estrogen and a major ingredient of most over-the-counter contraceptives [5].

Endocrine disruptors are considered disruptors, not only by their chemical nature but rather, by their biological significance and their impact on different organisms. Research supported by data has indicated that endocrine disrupting compounds have been linked to reproductive abnormalities in aquatic species [5, 6], complete impairment of the reproductive cycle in mammalian species [6, 7, 10], alteration of male characteristic, and carcinogenicity [11] hence, estrogens are categorized as major contributors to ecosystem imbalances [4, 5, 10, 12–14]. Research has also indicted that elevated estrogen levels have the ability to induce abnormal proliferation of cancerous cells, and has been linked to breast and lung cancer [2]. Regardless, physiological benefits and properties of estrogens such as 17β-estradiol have provoked medicinal researchers to establish estrogen therapies. For instance, hormonal replacement therapy (HRT) is a continuous therapeutic process prescribed for treatment of menopause symptoms through use of a combination of estrogens including 17β-estradiol in woman [15, 16] and has been popularized and recommended by medical practices on a global scale. Although HRT has been proven to have health benefits, the over-accumulation of estrogens during HRT treatment has been linked to augmentation, progression of cancerous cells and cardiovascular diseases in patient above the age of 60 [16]. The inevitable growing use of steroid hormones in many agronomic and health

interrelated sectors has resulted in their significant prevalence in the environment. Estrogen are mostly released through human and animal urine or waste [14, 17], released from dairy (i.e., eggs and milk) processing amenities and waste [18, 19]. These sources significantly affect the already compromised quality of municipal water, the ecological system and are major 17β-estradiol exposure pathways. Hence, estrogens are frequently released into the environment through domestic wastewater and effluents from agronomic industries.

The precarious challenge is that most steroid hormones such as 17β-estradiol are not completely catabolized or metabolized in the liver [20], eventually these chemical species are released as discharges into the wastewater systems, resulting in estrogen dissemination, accumulation, and contamination. Hence, there is a great need for simple, modern, rapid, and sensitive sensing tools, such as the one developed, to give insights and to screen the prevalence of estrogens in the environment, especially 17β-estradiol compound. Conventional wastewater treatment plants are not customized to completely eliminate estrogens, and they potentially leach-off into drinking water supplies. The elimination of the estrogenic endocrine disruptors in the environment depend on many factors such as the plant treatment mechanisms or water reclamation methods [21–23]. Wastewater treatment plants have been designed to remove estrogenic disruptors but 100% removal efficiency is still an obstinate target during water reclamation. Water is defined as the ultimate carrier of many pollutants and other hazardous substances including exogenous endocrine disruptors, making the effects of estrogenic endocrine-disrupting compounds prominent in our ecosystem. Monitoring the trace concentration levels of endocrine-disrupting compounds

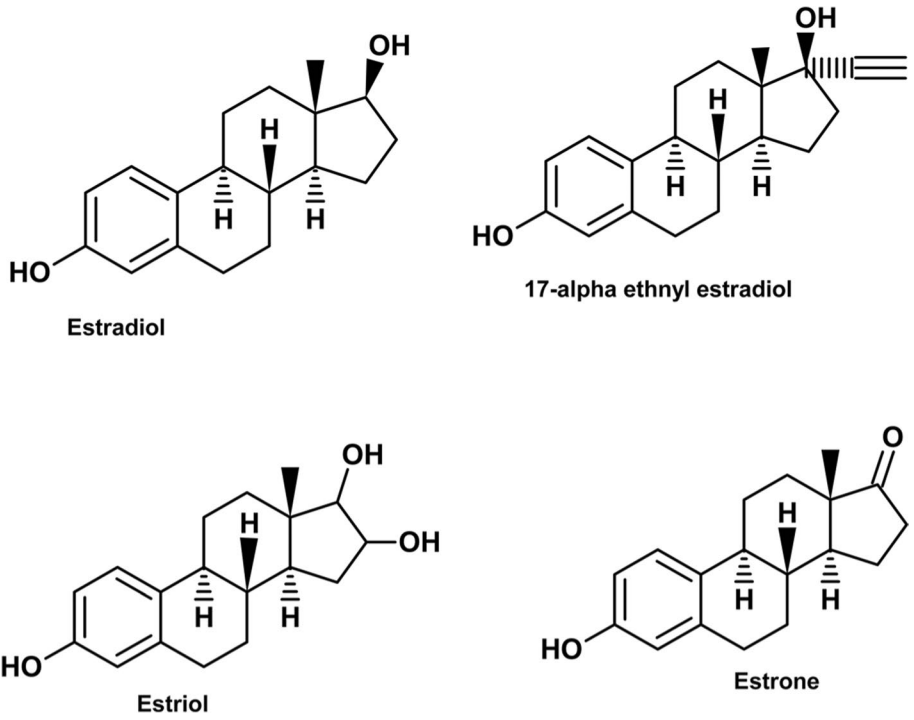

Fig. 1 Four main examples of estrogenic endocrine-disrupting compounds (e-EDC), 17β-estradiol, estriol, estrone, and synthetic estrogen 17α-ethynylestradiol

is crucial for instance, for quantifying the efficacy and effectiveness of different treatment methods and for profiling and tracking the full life cycle of endocrine disruptors and other toxic pollutants. 17β-estradiol possesses major health risks to both human life and other species. Henceforth, its prevalence in the environment can compromise the supply of quality drinking water, as many of the existing technologies are not designated to completely remove 17β-estradiol. Studies have indicated that drinking water supplies such as tap water and river water contain significantly low concentrations of 17β-estradiol [24, 25], which is cause for concern. These observations are reliant on many factors, such as age, demographics, and population dynamics contributing to wastewater and so forth. Profiling and mapping the occurrence of 17β-estradiol in different environments and population settings plays a pivotal role in understanding their transport mechanism in order to track their life cycle. Consequently, in order to develop and improve water reclamation procedures with highest removal efficiencies for estrogens or 17β-estradiol specifically, as it possesses the high disruption potency compared to other estrogens. A study on effects of 17β-estradiol on different aquatic species indicated that concentrations from 0.02 nM and above 1.3 nM of 17β-estradiol can cause abnormal sex differentiation ratios and reproductive abnormalities to aquatic species over a long-term exposure [24].

Detection of 17β-estradiol is currently achieved through techniques such as chromatography [10, 17], electroluminescence biosensing, and ELISA [26]. These techniques have great accuracy and sensitivity [2] in the same degree they are complex, bulky and require highly skilled operators for processing data analytics [1]. Electrochemical bio-sensing technologies for 17β-estradiol on the other hand can be effortlessly simulated and optimized to possess supplementary advantages such as being simple, portable, yet maintaining the same level of sensitivity, rapid detection, and accuracy. Electrochemical bio-sensors can also be miniaturized and configured into portable user-friendly devices to detect a range of compounds and pollutants. Chang Zhu and co-workers recently developed a highly sensitive electrochemical aptamer-based biosensor for 17β-estradiol using graphene grafted electrodes [27]. In another work, Kamila Spychalska and co-workers developed an enzyme-based biosensor for 17β-estradiol using poly(4,7-bis(5-(3,4-ethylenedioxythiophene) thiophen-2-yl)benzothiadiazole) and HRP enzyme, the biosensor demonstrated good sensitivity, selectivity, and a wide dynamic linear range [7]. Normazida Rozi and co-workers recently developed and reported an electrochemical aptameric biosensor for 17β-estradiol. The 73mer aptamer was conjugated and immobilized onto the poly(pyrole-co-pyrole-3-carboxylic acid) copolymer attached onto a screen-printed electrode. The immobilization of the polymer on the electrode surface significantly improved the conductivity of the bare electrode measurable by the low charge transfer resistance [28]. Although aptameric based electrochemical biosensing systems demonstrate good sensitivity and selectivity towards the detection of 17β-estradiol, aptamer bio-receptors are produced through complex and time-insensitive techniques such as selective evolution of ligands by exponential enrichment (SELEX).

Amongst many metal chalcogenide, ZnSe quantum dots in particular have been well explored in applications such as photo-catalysis [29], due to their size-dependent and tuneable opto-electronic properties. However, due to their interesting and a wide band gap energy of 2.7 eV [30], they could also be ideal platforms for tunneling electrons, due to presence of defected charge carrier sites in their crystal structures. Particle size diameters of quantum dots can vary from 2 to10 nm [31]. The small sizes of quantum dots could be translated into enhanced surface area to volume ratio hence enhanced surface reactivity. Quantum dots (QDs) can also be conjugated to complex micro-structures or biomolecules such as enzymes, peptides, antibodies, antigens, aptamers, DNA/RNA fragments, and cells,

for various nano-biosensing applications [32]. Compared to other metal chalcogenide and binary quantum dot systems, ZnSe nanocrystals possess better advantages such as being simple to produce. They are also fabricated from cost-efficient, environmental friendly, and non-toxic elements such as zinc metal-ions and selenide ions. Quantum dots can be reinforced or blended with conducting polymers for the development of opto-electrical devices and electrochemical sensing applications, and for establishment of other new properties and applications. The blending of quantum dots with conducting polymers could drastically improve for instance their electrical conductivity and charge carrier concentrations. There are several well-researched techniques for preparing quantum dot-polymer nanocomposites, such as drop-casting, surface passivation, covalent coupling, chain-end attachment layer by layer assembly, and direct grafting of quantum dots into polymers [33–36].

Polyaniline (PANI) is known for its remarkable electrical conductivity; this is attributed to its cyclic conjugated π-π bond system and the presence of amine polarons [37], making it a preferred material choice for various electrochemical applications. In addition, PANI possesses good environmental stability, high mechanical strength, and has high surface area [38]. PANI can be produced through simple methods such as chemical oxidation of its monomer and aniline in the presence of a strong oxidizing agents such as ammonia persulfate (APS); moreover, conducting polymers such as PANI can be produced through electrochemical induced polymerization (i.e., electro-polymerization) of the aniline monomer [38–44].

Hydrogen peroxidases (HRP) from the superfamily of peroxidase [45] and cytochromes P450 enzymes [46–48] are both heme group-containing isozymes even though the arrangements of their α-helix, β-sheet, and amino acid groups on the active site are contrast. HRP hemeprotein functions by generating reactive oxygen radicals at the iron-histidine-linked catalytic site [49] that subsequently react with various peroxidase substrates and are types of oxido-reductase enzymes [50]. Meanwhile, cytochromes P450 enzymes function by incorporating oxygen molecules into organic compounds and other substrates using the reactive iron-cysteine complex active site, hence are called heme-cysteine monooxygenases [51]. In particular, cytochrome P450 3A4 enzymes have shown to have high efficiency to metabolize and detoxify many xenobiotic compounds [47]; it is often obtained through manipulation of fauna species. Undifferentiated from cytochrome P450 enzymes, HRP can also mediate and catalyze the hydroxylation of organic compounds [52]. Compared to other enzymes expressed from complex organism, hydrogen peroxidase can be mostly extracted from root horseradish [53], isolated from plants [54], hence its extraction approach is much more sustainable. Peroxidase enzyme which is a type of hemeproteins does not only catalyze the oxidation of H_2O_2, but can be modified on electrode surfaces for electro-catalysis of other substrates such as hydro-peroxides, aromatic amines, organic hydro-peroxides, and a range of phenolic compounds [55]; this could also include xenobiotic compounds. The electron transfer kinetics occurring at the enzymes and proteins is an interesting concept that could be used to discover and understand many physiological redox processes [56]. This is done through modification of electrode surfaces with enzymes and proteins, a founding principle of biosensors and bioreactors.

Researchers Monireh Besharati Vineh and co-workers immobilized HRP enzyme onto functionalized reduced graphene oxide-SiO_2 nanocomposite and successfully used the platform to decompose various dyes and phenols [57]. Ru Xu in another study, immobilized the HRP enzyme onto the electrospun poly(methyl methacrylate-co-ethyl acrylate) microfibers for degradation and adsorption of bisphenol A [53].

In this work, a polyaniline (PANI)/3-mercaptopropionic acid capped zinc selenide quantum dots (3MPA-ZnSeQDs) nanocomposite was produced through a straightforward

entrapment of the 3MPA-ZnSe quantum dots into PANI during electro-polymerization of aniline. Due to their narrow bandgap, ZnSe quantum dots exhibit intermediate electrochemical properties, in the same manner attributable to its excellent conductivity: PANI was introduced to improve the overall electrochemical conductivity of the bio-sensing electrode. The 3-mercaptopropionic acid capping ligand on the surface of ZnSe quantum dots enhanced the susceptibility of the mediator film to bind to HRP enzyme, used as the bioreceptor. The PANI:3MPA-ZnSeQD nanocomposite did not only facilitate the transfer of electrons during the detection of the target analyte, but also played a significant role in enhancing the sensitivity of the bio-sensing platform. Nano-sized quantum dots allowed for high loading of the enzyme onto the sensing electrode, making it compatible for its intended bio-sensing application. This is attributable to both their high surface area to volume and the chemical functionalities of the capping ligand around the surface of the ZnSe quantum dots. For the first time, we report a horseradish peroxidase (HRP) enzyme integrated onto the PANI:3MPA-ZnSeQD nanocomposite to fabricate a biosensor to detect 17β-estradiol. The PANI:3MPA-ZnSeQD/HRP-based electrochemical biosensor demonstrated excellent sensitivity, a significantly low detection limit, and high binding efficacy towards 17β-estradiol. Horseradish peroxidase enzyme is well known to catalyze the oxidation of peroxides. However, in this study, we demonstrated that a blend of horseradish peroxidase with PANI:3MPA-ZnSeQD nanocomposite could be a potential coenzyme material to not only expedite the effective electron transport but the HRP/quantum dot polymeric nanocomposite blend efficiently catalyzed the oxidation of preferable 17β-estradiol. The binding kinetics and mechanism of the HRP enzymes immobilized on the electrode surface upon its interaction with 17β-estradiol were used to establish biosensor parameters such as binding efficacy to the analyte of interest. The developed nanobiosensor parameters were benchmarked and comparable to assays and biosensors reported in literature, the biosensor had an added benefit of being straightforward and miniaturize-able.

Materials and Methods

Materials

All chemicals used in this study were of analytical grade and purchased from Merck (Johannesburg, South Africa). This include sodium phosphate monobasic anhydrous ≥ 98%, sodium phosphate dibasic anhydrous ≥ 98%, zinc nitrate hexahydrate 98%, selenium powder 99.99%, trace metal basis, sodium borohydride 99.99% trace metal basis, 3-mercaptopropionic acid (3MPA) ≥ 99%, sodium hydroxide ≥ 97%, aniline 99.5%, hydrochloric acid 37%, potassium hexacyanoferrate(II) trihydrate ≥ 99.95%, potassium hexacynaferrate (III) ≥ 99%, horseradish peroxidase (HRP) {type VI, essentially salt free, ≥ 250 units/mg solid, EC 1.11.1.7}, bovine serum albumin (BSA) {lyophilized powder, crystallized ≥ 98.0%, glutaraldehyde solution 50%, 17β-estadiol ≥ 98%, 17α-ethynylestradiol ≥ 98%, estrone ≥ 99%, and ethylenediaminetetraacetic acid (EDTA) 99.4–100.6%}. The 0.1 M phosphate buffer solutions (PBS) of pH 7.4 were prepared from sodium phosphate monobasic anhydrous and sodium phosphate dibasic anhydrous using ultrapure water filtered by Ris-millipore filtering system. The 50% glutaraldehyde solution was used as the binder to attach the HRP enzyme on nanocomposite-modified electrode, BSA was used to control-unspecific binding.

Methods

Instrumentation

Transmission electron microscopy (TEM) images and energy dispersive X-Ray (EDX) spectra were recorded on a Tecnai G2 F20X-Twin MAT 200-kV Field Emission Transmission Electron Microscope from {Field Electron and Ion (FEI) Company Hillsboro, OR, USA}. Fourier transform infrared (FT-IR) spectra were recorded on a 100 FT-IR spectrometer (PerkinElmer Incorporated, Waltham, MA, USA). The ultraviolet–visible (UV–Vis) spectrums were done in quartz cuvettes on Nicolet Evolution, 100 UV–visible spectrophotometer (Thermo Electron Corporation, Waltham, MA, USA). All voltammetry experiments were carried out with a BAS 100 W Electrochemical Analyzer {Bioanalytical Systems Incorporated (BASi), West Lafayette, IN, USA}. The Nyquist plots were recorded on an Autolab PGSTAT 320 N potentiostat/galvanostat (Metrohm, Cape Town, South Africa) operated using Voltalab version 4 software. The electrochemical impedance spectroscopy (EIS) data was fitted and simulated using ZView software.

Synthesis of 3-Mercaptopropionic Acid-Capped ZnSe Quantum Dots

Briefly, 0.03 g zinc nitrate hexahydrate salt was dissolved in 50 mL ultrapure water consisting of 69.9 µL of 3-mercaptopropionic acid (3MPA). The pH of the resulting solution was then adjusted to 8 using 0.1 M NaOH. The solution was then stirred under N_2 saturated atmosphere for 2 h at 25 °C. After which, 10 mL of 0.02 M selenium ions (i.e., prepared by chemical reduction of 0.2 mmol selenium powder by equivalent molar of $NaBH_4$) was slowly introduced using a micro-syringe. The quantum dots were then allowed to nucleate for 1 h at 25 °C, under inert atmosphere. The resulting 3-mercaptopropionic acid-capped ZnSe quantum dot (3MPA-ZnSeQD) solution was immediately transferred into the refrigerator, at − 20 °C for 5 min to quench the size escalation. The water-soluble 3MPA-ZnSeQD final solution was then washed with absolute ethanol through centrifugation at 5000 rpm. The as-prepared 3MPA-ZnSeQD nanomaterials were stable for several days when kept at 4 °C.

Electrochemical Synthesis of PANI

The electro-polymerization or electrochemical synthesis of PANI was performed on a gold electrode surface. A potential window between 1100 and − 200 mV and a scan rate of 100 mV s^{-1} were used. Ten voltammetric cycles were performed in an inert solution containing 3000 µL of 0.1 M aniline and 1 mL of 1 M HCl. The formation of PANI onto the surface of the gold electrode was attested by cyclic voltammetry (i.e., shown in the supplementary material, Fig S1 A) and the appearance of the emerald base derivative of PANI onto the working electrode surface. In order to etch-off and re-disperse the PANI, for ex situ analysis, the gold electrode surface modified with PANI was immersed into an absolute ethanol solution.

Preparation of the PANI:3MPA-ZnSeQD Nanocomposite

Similar to the "Electrochemical Synthesis of PANI" section, cyclic voltammetry was used to prepare the polyaniline: 3MPA-ZnSe quantum dot nanocomposite. The

parameters were kept consistent as previous. A gold disk electrode was immersed in a solution containing: 3000 µL, of 0.1 M aniline solution, and 40 µL of the 3MPA-ZnSeQD nanomaterials in 960 µL of 1 M HCl. Then after, 10 cyclic voltammetry scans were performed at 100 mV/s, at a potential window between 1100 and − 200 mV. The resulting PANI:3MPA-ZnSeQD nanocomposite-modified gold electrode surface was washed with de-ionized water to remove unreacted or unbound residues of aniline. Manelahalli and co-workers mentioned that the doping of PANI could be achieved using many approaches, one strategy being doping of the PANI during electrochemical polymerization. This is done by creating inter p-doped and n-doped states on the surface of the polymer [58]. These are anticipated then to interact with either n- or p-states of the dopant. In our case, the carboxylate ion provides negative surface charges that could effortlessly interact with p-doped $NH^{\delta+}$ states of the polyaniline, providing a very stable interaction. The formation of the PANI:3MPA-ZnSeQD nanocomposite was also attested by cyclic voltammetry characterization displayed in the supplementary material, Fig S1 B.

Fabrication of the AuE/PANI:3MPA-ZnSeQD/HRP Biosensor Electrode

The HRP enzyme was introduced onto the PANI:3MPA-ZnSeQD-modified electrode by drop-casting of 2 µL of the 2.8×10^{-5} M HRP. Precisely, 0.2 µL of 2% glutaraldehyde solution was used as the binder to crosslink the HRP enzyme molecules with the PANI:3MPA-ZnSeQDs modified on the gold electrode surface. This was done to achieve adequately enhanced stability of the enzyme biomolecule on the surface of the transducer. The HRP enzyme in this case is expected to covalently attach to the surface of the nanocomposite through its N-terminus/amine amino acids via amine and carboxylic acid functional groups from the PANI:3MPA-ZnSeQD nanocomposite by means of glutaraldehyde cross-linking strategy. The partial negative charges on the carboxylate ion functional groups from the capping ligand of quantum dots dissipate the charge along the polymer matrix in order to create sites for electrostatic attachment of the HRP enzyme molecules. The AuE/PANI:3MPA-ZnSeQD/HRP biosensor electrode was then carefully washed with ultra-pure water to remove any unbound molecules. Then after, 2µL of bovine serum albumin (BSA) solution was drop-cast onto the AuE/PANI:3MPA-ZnSeQD/HRP-modified electrode surface to control the un-specific binding, through insulation of the bare or exposed gold electrode sites. The AuE/PANI:3MPA-ZnSeQD/HRP biosensor was then used for electrochemical characterization and analysis. A schematic illustration in Fig. 2 demonstrates the development of an AuE/PANI:3MPA-ZnSeQD/HRP biosensor electrode for sensing the 17β-estradiol (E2) compound.

Preparation Of Real Samples

Real samples were prepared by spiking different concentrations (0, 2, and 3 µM) of 17β-estradiol into tap water. No further pre-treatment step for the prepared samples was required. Two hundred microliters of tap water samples and 200 µL of 0.1 M phosphate buffer solution of pH 7.4 were efficiently mixed using a Votex^{Tm} shaker for 3 min at 5000 rpm. Then after, the prepared 17β-estradiol-spiked samples were analyzed using the developed bio-sensing electrochemical method.

Results and Discussion

Chemical Structure Analysis

The FT-IR spectrum of the PANi:ZnSeQDs with different ratios of aniline to 3-mercaptoproinic acid capped ZnSe quantum dots is shown in Fig. 3a. The aniline:ZnSe quantum dot ratios of 1:1, 1:2, 1:4, 2:1, and 4:1 resembled very similar spectra attributed to similarity in the conservation and distribution of the chemical functional groups. However, a good distribution of functional groups from both PANi and 3MPA-ZnSe quantum dots were obtained when the ratio of the polyaniline and 3MPA-ZnSe quantum dots was 1:2, as seen in Fig. 3a. This is evidenced by high transmission percentages attained compared to other ratios, entailing exposure of a high degree of chemical functionalities, with limited shielding effect from either PANI or 3MPA-ZnSeQD nanomaterials.

As exhibited in the spectrum demonstrated in Fig. 3b, the strong to medium bands at 2901 cm^{-1} and 1560 cm^{-1} in the spectrum of PANI are a characteristic of C-H stretch and C = C vibrational stretch of the benzenoid ring [59] respectively, while the bands observed at 1243 cm^{-1} and 1000 cm^{-1} could be assigned to the vibrational stretch of the C-N bond of the benzonoid ring and C-H in-plane bending mode from the aromatic ring respectively [60].

The presence of the 3-mercaptopropionic acid capping ligand on the surface of the ZnSe quantum dots was evidenced by the appearance of a strong to medium vibrational bands at 3276, 1590, 1339 cm^{-1}, and 831 cm^{-1} indexed in the spectrum displayed in Fig. 3b). These stretching frequencies are attributed to vibrational bands of O–H. C = O,

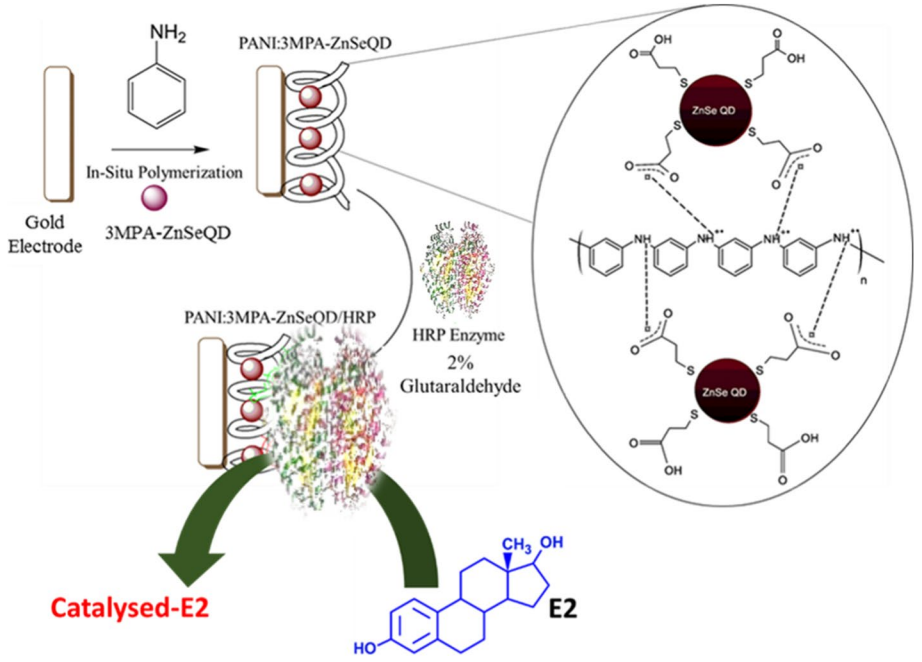

Fig. 2 Schematic representation of the development of the AuE/PANI:3MPA-ZnSeQD/HRP biosensing electrode

O–H bending, and C-H bending modes from the 3-mercaptopropionic acid, respectively. The attachment of the 3-mercaptopropionic acid ligand on the surface of the quantum dot core indeed occurred through the thiol terminus functional group which interacted with the Zn metal center of the ZnSe quantum dots. This was affirmed by the appearance of the metal-sulfide strong vibrational band at 662 cm^{-1} (i.e., Zn–S bond in this case) [60, 61].

There was no significant change in the chemical structure of the emerald salt of PANI upon doping with 3MPA-ZnSe quantum dots as indicated by the FTIR spectrum presented in Fig. 3b. The FTIR indicated a strong evidence of the presence of both 3MPA-ZnSe quantum dots and nanostructured PANI. However, what was interesting to note was that there was an appearance of the new asymmetric $\nu(C=O)$ strong band at 1644 cm^{-1}. A significant shift in the appearance of the $\nu(C=O)$ vibrational frequency may also indicate the conversion of the carboxylic acid functional group into an amide functional group. This could have been facilitated by the amine functional groups from polyaniline and the carboxylic acid functional groups from the 3MPA capping ligand from the ZnSe quantum dots. The shift in the vibrational stretching frequency $\nu(C=O)$ however provides a strong evidence of a strong interaction that occurred between the quantum dots and the polyaniline.

Size and Morphology Studies

To confirm the formation of the nanocomposite, morphology, and particle size distribution of the materials, 3MPA-ZnSeQDs, PANI, and PANI:3MPA-ZnSeQD materials were examined using transmission electron microscopy (TEM) analysis coupled to an energy dispersive X-Ray (EDX) analyzer. Figure 4A, C, and E represent the obtained TEM images for 3MPA-ZnSeQD nanomaterials, PANI, and PANI:3MPA-ZnSeQD composite, respectively. The corresponding EDX spectra are displayed in Fig. 4B, D, and F. Figure 4A demonstrates that the 3MPA-ZnSe quantum dot nanomaterials had an average particle size (APS) of 5.3 ± 0.93 nm. The EDX elemental analysis in Fig. 4B confirmed a good distribution of both the Zn and Se atoms in the ZnSe quantum dots, in addition confirmed the presence of a significant percentage of C, H, and S elements resulting from the 3-mercaptopropionic acid capping ligand. The 3MPA-ZnSe quantum dots were mono-dispersed with minimal agglomeration. The agglomeration effect demonstrated by the 3MPA-ZnSe quantum dots was also observed by Uzma Menon and co-workers when investigating the morphological features of ZnSe quantum dots with different stoichiometry [62]. The effect of aggregation could also be influenced by the size or length of the alkyl chain of the capping ligand. Nano-sized quantum dots have much more improved surface area to volume ratio [60], hence have the ability to efficiently enhance the surface area of the composite and are good platforms to capture a significant degree of enzyme biomolecules on the bio-transducer surface. This interaction is also facilitated by the distribution of the conserved functional groups from the capping ligand of the quantum dots that are often utilized as cross-linkers to immobilize biomolecules such as enzymes. TEM studies of PANI in Fig. 4C, demonstrated nanofibers arranged in a form of a network structure. The thicknesses of the as-synthesized PANI fibers was measured to be approximately 40 nm. The EDX spectrum of PANI demonstrated the presence of high percentage of C attributable to the carbon atoms of the polyaniline. The significant percentage of oxygen elements is due to the adsorbed methanol solvent matrices, used as the polymer dispersant.

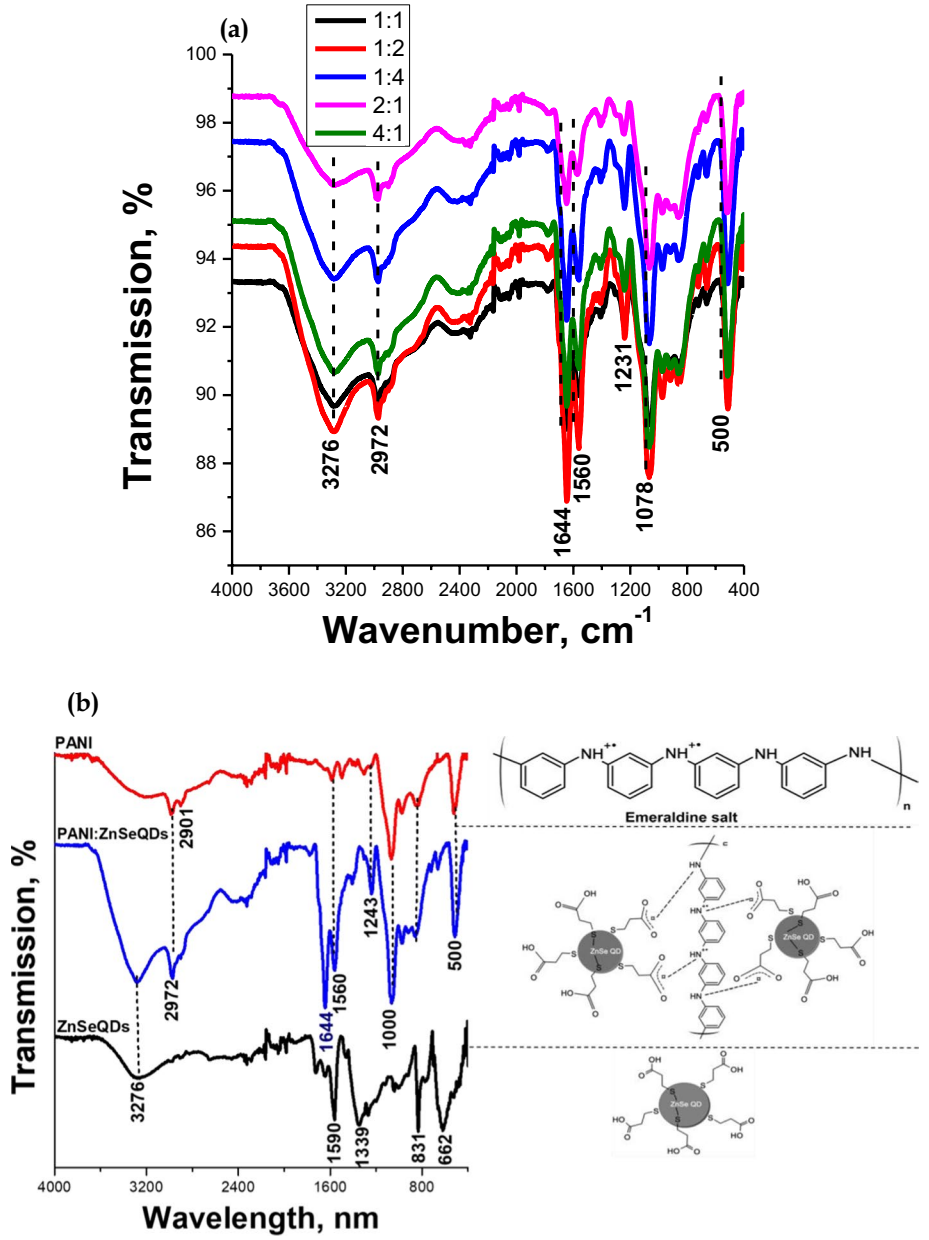

Fig. 3 **a** The FTIR spectra of PANI:3MPA-ZnSeQD nanocomposite at different rations of PANI and 3MPA-ZnSeQDs. **b** The FTIR spectra of PANI and 3MPA-ZnSeQD nanomaterials and PANI:3MPA-ZnSeQD composite

As seen in the TEM image represented by Fig. 4E, the quantum dot nanocrystals were evidently bound or adhered onto the polymer fibers. Subsequently, 3MPA-ZnSe nanoparticles were well distributed onto the surface of PANI, evidencing the successful

formation of the polyaniline:3MPA-ZnSe quantum dot nanocomposite. Adherence of the 3MPA-ZnSe quantum dots onto the polyaniline had inconsequential effect on the quantum dot nano-crystallite sizes. The presence of the 3MPA-ZnSe quantum dots onto the PANI fibers was also evidenced by the EDX analysis shown in Fig. 4F. The EDX spectrum of the PANI:3MPA-ZnSeQD nanocomposite evidenced the presence of a percentage of element C, O, S, Zn, and Se assigned to both the presence of the polyaniline and 3MPA-ZnSe quantum dots. Although the EDX spectrum of the composite PANI:3MPA-ZnSeQDs resembles that of the PANI alone, the intensity of the C atoms was higher, further reinforcing the presence of the polyaniline. The presence of PANI fibers within the composite was however very evident based on the presented corresponding TEM image. The successful incorporation of the 3MPA-ZnSeQDs onto the polyaniline network was also confirmed by the electrochemical characterization (i.e., alluded to in Sect. 1.1 of the supplementary document) of the PANI before and after incorporation of the quantum dots, which yielded significantly divergent electrochemical behavior. Chaitanya and co-workers mentioned that a combination of polymer network and quantum dots is envisioned to have improved surface area, contributed by high surface area of the nanopolymer fibers and the small sized quantum dots [60]; this is also an ideally required property for its intended electrochemical application.

Opto-electrochemical Properties

The magnitude of the bandgap energy of nanomaterials and materials could be efficiently employed to predict their redox behavior. Optical band gap energies (E_g)s of (I)PANI, (II) 3MPA-ZnSe quantum dots and (III) PANI:3MPA-ZnSe nanocomposite were estimated from the absorbance energy bands using Tauc's photon energy approximation, which relates the nanomaterial's optical properties to its photon energy properties. Tauc's equation is presented by Eq. (1) [63–66].

$$\alpha h\nu = c\left(hv - E_g\right)^{1/2} \tag{1}$$

In the equation, α is the absorption co-efficient, h is the Planks constant, ν is the frequency of the absorbed photons, c is the speed of light, and E_g is the photon band gap energy. The x-intercept of Taucs's plot designates the indirect band gap of a semiconductor or conducting material. The nanomaterials; PANI, 3MPA-ZnSeQD, and PANI:3MPA-ZnSeQD nanocomposite had band gap energies of 3.82, 4.4, and 4.5 eV respectively estimated from Tauc's plots illustrated in Fig. 5A. The presence of 3MPA-ZnSeQD nanomaterials within PANI significantly increased its indirect band gap energy by 0.58 eV. This could be attributable to the incomplete electron–hole recombination process [67], due to the availability of other higher energy inter-conduction bands contributed by the quantum dots. Hence an increased energy gap which could be translated to the reduction in the electron conductivity was observed. This phenomenon could be ascribed to the semiconducting nature of the 3MPA-ZnSe quantum dots.

To understand the redox behavior of the as-produced materials, electrochemical impedance spectroscopy (EIS) study was performed on the standard three-electrode system in an electrolyte solution containing two redox active probes: 5 mM $Fe(CN)_6^{3-}$ and 5 mM $Fe(CN)_6^{4-}$ in 0.1 M PBS. For EIS studies, an applied formal potential ($E^{0'}$) of 204 mV in a single step mode between the impedance frequency range of 1 MHz to 1 kHz was applied. The EIS is capable of determining charge susceptibility of modified surfaces in relation

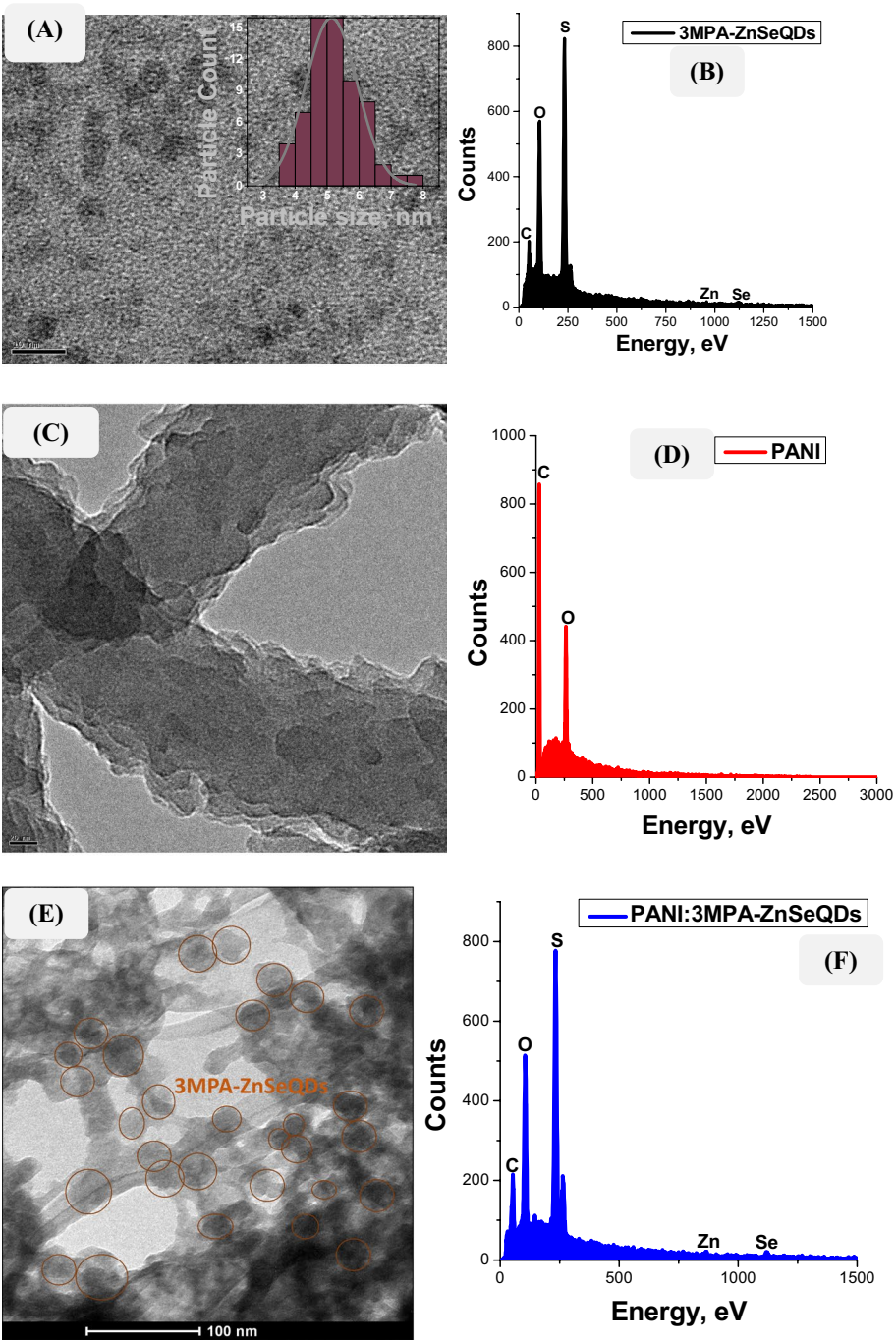

Fig. 4 **A** TEM micrographs of 3MPA-ZnSe quantum dots. **B** Particle size distribution profile of 3MPA-ZnSeQD. **C** and **D** TEM micrographs of PANI and PANI:3MPA-ZnSeQD nanocomposite

to the electrode/electrolyte interfaces. The charge transfer properties of polyanaline nanocomposites could be effortlessly determined through evaluation and monitoring of charge transfer resistances (R_{ct}), represented by the semi-circles of the Nyquist plots at high frequencies and the Warburg diffusion process occurring at low frequencies [44]. The EIS Nyquist plots are shown in Fig. 5B, the data was fitted using Z_{view}^{TM} software to estimate the R_{ct} values. The Nyquist plots of 3MPA-ZnSe quantum dot-modified gold electrode surface revealed the highest charge transfer resistance; R_{ct} of 6 kΩ, followed by the unmodified gold electrode with the R_{ct} magnitude of approximately 3.3 kΩ. The variation in the R_{ct} values after the electrode modification process with the two materials also confirmed the successful mobilization of the electrode surface with the specified nanomaterials. The R_{ct} of the PANI:3MPA-ZnSeQD nanocomposite films-modified gold electrode showed a charge resistance R_{ct} of 1.25 kΩ; this was the lowest charge transfer resistance amongst the studied materials. Modification of the electrode surface with PANI:3MPA-ZnSeQD films improved the charge transfer redox properties of the electrode surface, hence improved its capacitive behavior, electron channel and conductivity. This is as a consequence of the presence of a highly conductive PANI within the nanocomposite, which has negligible charge transfer resistance in ferric/ferro-cyanide probe. Hence, the assumption that PANI improves the overall conductivity of the platform was consistent with EIS data. The surface

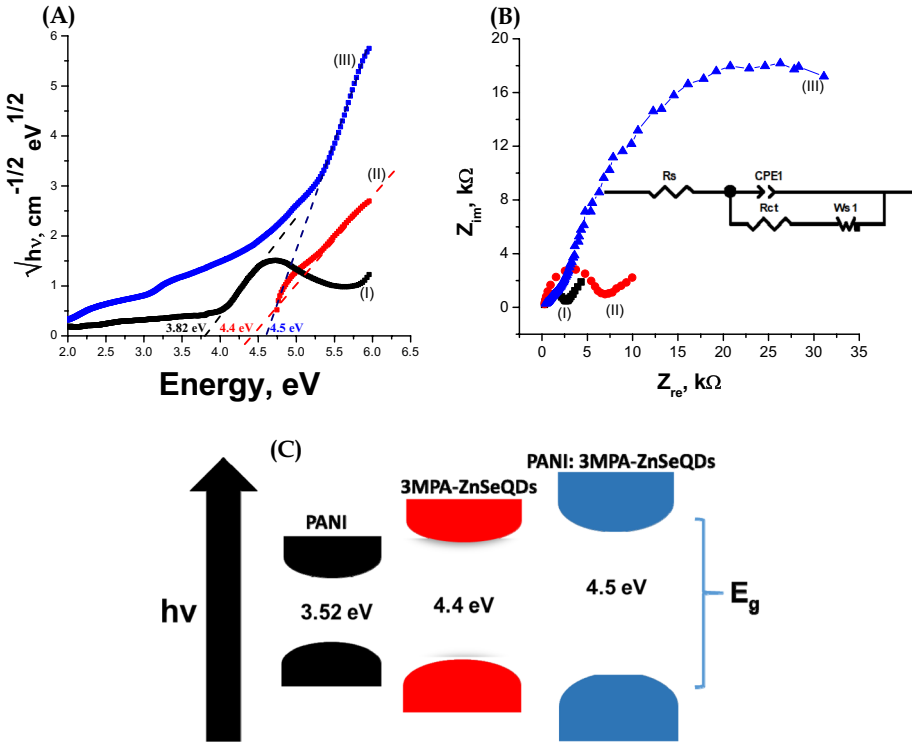

Fig. 5 **A** Tauc's plot of bare (I) PANI, (II) 3MPA-ZnSeQD nanomaterials, and (III) PANI:3MPA-ZnSeQD (P:QD) composite. **B** The corresponding Nyquist plots of (I) bare gold electrode (II) 3MPA-ZnSeQD, and (II) AuE/PANI:3MPA-ZnSeQD-modified electrodes in $K_3Fe(CN)_6$ and $K_4Fe(CN)_6$ redox probe and 0.1 M phosphate buffer solution (PBS). **C** Corresponding band gap representation

coverages of the films on the electrode surface were estimated using Eqs. (2) and (3) relating the charge transfer resistances (R_{ct}) with the electrode surface coverages (θ) [68]:

For 3MPA-ZnSeQD nanomaterials modified on the gold electrode:

$$\theta = \left| 1 - \frac{R_{ct}^{bare}}{R_{ct}^{AuE/3MPA-ZnSeQD}} \right| \quad (2)$$

For the PANI:3MPA-ZnSeQD composite films modified on the gold electrode:

$$\theta = \left| 1 - \frac{R_{ct}^{bare}}{R_{ct}^{AuE/PANI3MPA-ZnSeQD}} \right| \quad (3)$$

The parameter θ is the surface coverage, R_{ct}^{bare}, is the charge transfer resistance of the bare gold electrode, $R_{ct}^{3MPA-ZnSeQD}$ and $R_{ct}^{PANI:3MPA-ZnSeQD}$, are charge transfer resistances of the 3MPA-ZnSe quantum dots and PANI:3MPA-ZnSeQD nanocomposite-modified gold electrodes respectively. The surface coverage, θ of the; 3MPA-ZnSeQD nonmaterial and PANI:3MPA-ZnSeQD-modified gold electrodes were found to be 4.5 and 1.461 respectively. A low surface coverage could be an indication of a typical thinner layer covering on the electrode surface, thus faster exchange of charged species (i.e. ions) and electrons within the electrode's capacitive and diffusion layer. This then affirms that the PANI:3MPA-ZnSeQD nanocomposite was the most efficient and highly conducting material, hence an excellent mediator for the effective ion and electron permeation on the electrode interface.

The Analytical Performance of the AuE/PANI:3MPA-ZnSeQD/HRP Biosensor

Detecting 17β-estradiol at even its sub-zero concentrations is mandatory for the sustainability of our ecosystem and for maintaining high drinking water standards. The performance of the designed biosensor was evaluated using differential-pulse voltammetry (DPV). The DPV measurements were carried out under aerobic and anaerobic conditions. Anaerobic conditions were achieved by degassing the phosphate buffer solution (PBS) for about 10 min with a purge of argon gas to remove the dissolved oxygen molecules and keeping an argon blanket on top of the solution during the analyte concentration measurements. For aerobic measurements, the degassing step was eliminated completely. The responses of the biosensor to 17β-estradiol (E2) were monitored and recorded at a potential window between − 600 and 400 mV. The developed biosensor electrode responses increased linearly and proportionally with increasing concentrations of 17β-estradiol from concentrations between 0.5 and 4 µM, as depicted in Fig. 6A, measured at a formal peak potential (E_p) = − 163 ± 22 mV. This was an indication of a good affinity of the HRP mobilized on the electrode surface with analyte 17β-estradiol. This cathodic peak was suggested to be due to current response generated and induced by the electron, ion, or proton transfer reaction occurring at the biosensing electrode interface. In the same order, an insignificant cathodic potential shifts after continuous additions of 17β-estradiol were observed. The cathodic or anodic potential shift can often be contributed by the moderation of the oxidation state of the enzyme's active site or catalytic center. A linear regression equation for the calibration curve, shown in Fig. 6B, was determined to be I(µA) = 0.074(µA/µM) + 0.1(µA), R^2 = 0.98. The limit of detection (LOD) was calculated to be 0.2 µM

(S/N = 3). Oxygen poisoning is a very common adverted phenomenon in enzyme biosensors. This occurs when the bio-transducer interacts with the dissolved oxygen molecules, resulting in oxygen poisoning or adsorbed oxygen layer on the bio-transducer. Most enzyme have oxygen adsorption capabilities, capture dissolved oxygen molecules, and use them as co-modulators during catalysis of their substrates. The adsorption of oxygen molecules in a bio-transducer can result in loss of sensitivity and bio-receptor fouling [69]. However, the developed biosensor, AuE/PANI:3MPA-ZnSeQD/HRP electrode, was insignificantly affected by the presence of dissolved oxygen species as depicted in the catalytic DPV responses demonstrated by Fig. 6C and D. This could be attributed to mediating layer's ability to quench and reduce oxygen molecules, thus allowing solely electrons and protons/ion to channel or hop through the electrode's double-layer interface. Subsequently, oxygen molecules are also a pre-requisite to most HRP enzymatic reactions. This prediction is also revealed and referenced in the HRP catalytic mechanism illustrated in the "The AuE/PANI:3MPA-ZnSeQD/HRP Bio-sensor Electrode Mechanism" section. As demonstrated in Fig. 6C, the higher response currents were generated by the biosensor under aerobic conditions, hence an indication of a much more improved sensitivity. The sensitivity of the biosensor was increased from 0.074 to 0.5 μA/μM in the presence and absence of oxygen molecule in the electrolyte, respectively. The linear regression equation extrapolated from the calibration curve shown in Fig. 6C for the biosensor at aerobic conditions was I(μA) = 0.5(μA/μM) + 0.78(μA), $R^2 = 0.94$. Its dynamic linear range was determined to be from 0.5 to 2.5 μM, and an LOD of 0.03 μM ($S/N = 3$) was established. It is also important to note that the redox response peaks assigned to the interaction of the biosensor with the 17β-estradiol shifted to much lower redox potentials and were observed at the formal potentials (E_p) of − 25.7 ± 7.2 mV. Hence, it can be obviously concluded that the oxygen molecules drastically lowered the overall onset potential energy at which the 17β-estradiol is expected to be oxidized. Therefore, oxygen could be used as an efficient co-molecule to minimize the electrochemical energy demand of the electrolytic cell under study.

The electrochemical behavior of the biosensor towards different concentrations of 17β-estradiol at both conditions was further explained by the use of the fitted hill pseudo-hyperbolic curves and biosensor responses that are demonstrated in the graphs presented by Fig. 6B and D. The Michaelis–Menten model could be employed to estimate the enzyme–substrate binding kinetic behavior at the electrode surfaces and diagnose if the enzyme catalysis at the interface is the rate determining step [70]. Adopted from literature, the Michaelis–Menten model [71–73] in this case would be presented as highlighted in Eq. (4).

$$\mathrm{i_p} = \frac{\mathrm{i_{max}}\left[17\beta - \mathrm{estradiol}\right]}{\left[17\beta - \mathrm{estradiol}\right] + \mathrm{K_m}} \tag{4}$$

The parameter i_p are the peak currents, i_{max} is the maximum response current, [17β-estradiol] is the concentration of 17β-estradiol, and K_m is the substrate-enzyme binding affinity constant (i.e., the Michaelis–Menten constant). The Michaelis–Menten constant (K_m) describes the efficacy of the enzyme to catalyze a specific substrate. On a condition that the enzyme–substrate catalytic reaction occurring at the electrode interface is significantly fast, the response current signals are expected to conform to the Michaelis–Menten model [70]. The catalytic reaction between 17β-estradiol and HRP enzyme covalently bound onto the biosensor electrode interface fitted well with the modified kinetic model, however only at aerobic conditions. The K_m(s) and $i_{max}/2$ values were calculated to be 0.64 μM and 2.33 μA respectively. However, under anaerobic conditions, the

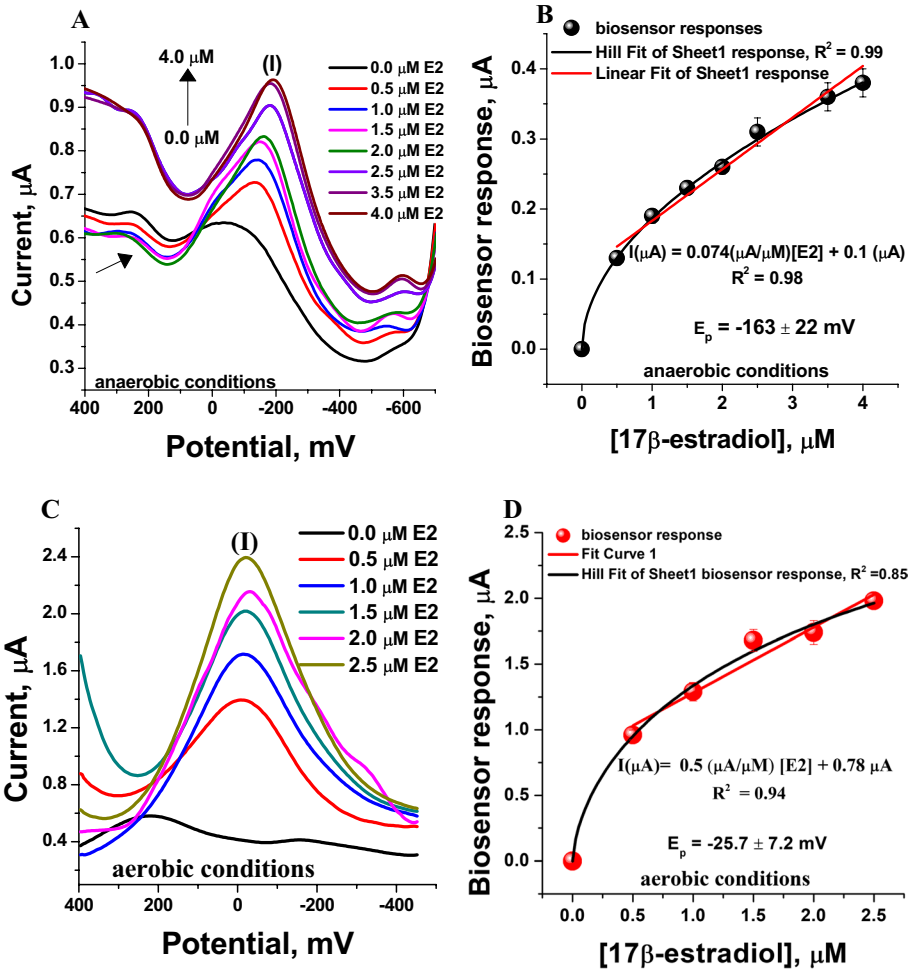

Fig. 6 **A** DPV responses and **B** corresponding calibration plot of the AuE/PANI:3MPA-ZnSeQD/HRP biosensor responses to successive addition of different 17β-estradiol (E2) concentrations {i.e., 0.0, 0.5, 1.0, 1.5, 2, 2.5, 3, 3.5, 4 μM} in 0.1 M phosphate buffer electrolyte solution, pH 7, under anaerobic **C** DPV responses and **D** corresponding calibration plot of the biosensor under aerobic conditions at {i.e., 0.0, 0.5, 1.0, 1.5, 2, 2.5 μM of 17β-estradiol}

catalytic reaction between the HRP enzyme and 17β-estradiol did not inevitably follow the Michaelis–Menten model, as significantly high values of the K_m and $i_{max}/2$ were obtained, despite that fact that the [17β-estradiol]-biosensor responses showed a strong indication of a pseudo-hyperbolic saturation behavior. The developed biosensor showed excellent electrochemical performance towards the detection of 17β-estradiol, and its sensing parameters was benchmarked against biosensors and assays reported in literature alluded to in Table 1. The sensitivity of the biosensor could however be drastically enriched by incorporating high concentrations of the HRP enzymes and the high concentration of the nanocomposite for further amplification of the electrochemical signal generated; however, thick electrode surfaces are mostly prone to electrode fouling.

The Specificity of the Biosensor

Selectivity of the biosensor is a very crucial parameter for the practical application of the biosensors and sensing devices. In order to establish whether the developed biosensor could mediate any catalytic change in the presence of similar compounds to 17β-estradiol, the differential pulse voltammetry responses of the biosensor to other estrogenic endocrine-disrupting compounds with high structural similarity index to 17β-estradiol were studied. The DPV responses are displayed in Fig. 7A to F. Compounds, estrone (E1), 17α-ethinylestradiol (EE2), and estriol (E3), were chosen and their structures are shown in Fig. 1, in the "Introduction" section. Ethnylestradiol-17α (EE2) is another type of synthetic-estrogen used as a major ingredient during production of female oral contraceptives-administered for birth control [3, 10, 14]. EE2 shares a similar structure with the E2; however, the hydrogen at the 17th carbon position of the estradiol is replaced by an additional carbon-linked alkyne group [10]. Estriol is characterized by the presence of additional OH functional groups at the 16th position of the E2 steroid backbone.

No successive catalytic responses were mediated by the biosensor in the presence of estrone (E1) at concentration above 0.5 μM in the electrolyte solution, as demonstrated in Fig. 7A and B. Due the similarity of estriol (E3) to 17β-estradiol, it was expected that the biosensor would be responsive towards E3, however, no concentration-dependent electroanalytical responses were observed for estriol (E3) as well, as indicated in Fig. 7C and D. Most often, the substrate initially interact with the enzyme's active site, mobilized on the electrode surface before any catalytic reaction is stimulated. This interaction occurs via hydrogen bonding with the corresponding amino acids at the enzymes active site, this is alluded to and referenced in details in the "The AuE/PANI:3MPA-ZnSeQD/HRP Bio-sensor Electrode Mechanism" section. Nevertheless, the hydroxyl functional group at the 16th position of the estriol steroid backbone might have sterically hindered the ability of the substrate to be hydroxylated. Hence, the active site is then expected to remain unchanged, and no enzyme catalytic reaction is expect to occur for that reason. It is interesting to note that the biosensor responded slightly good to addition of a single concentration of 17α-ethinylestradiol (i.e., 0.5 μM) at a formal potential of − 200 mV, as displayed by the DPV responses in Fig. 7E and F. At concentrations above 0.5 to 1.5 μM, the EE2 analyte induced concentration-dependent electroanalytical response signals at the formal potential (E_p) = − 62 mV. This could be attributable to the selectivity of the HRP bio-receptor (i.e., mobilized on the bio-transducer) to phenolic alcohols. HRP enzymes are well known to induce catalytic effect on substrates such as; aromatic alcohols, phenolic compounds, and peroxides [72, 73, 76]. Nonetheless, the redox potential induced by EE2 is however dissimilar to the reduction potential at which the electroanalytical responses of the biosensor towards 17β-estradiol were observed. Hence, the developed biosensor seemed to have a good preference towards successive addition of 17β-estradiol over other estrogenic endocrine-disrupting compounds, measureable at a distinct potential. Hence, possessed acceptable selectivity especially at concentrations of the analyte above 0.5 μM. The comparison of maximum biosensor responses to different estrogenic compounds are summarized in Fig. 7G.

Despite the fact that HRP enzyme immobilized on the developed biosensor surface efficiently catalyzed the oxidation of 17β-estradiol with high selectivity compared to other estrogenic endocrine-disrupting compounds, peroxide substrates such as hydrogen peroxide (H_2O_2) can potentially interfere with the electrocatalysis of 17β-estradiol. Hydrogen peroxide for instance has been an issue during water reclamation (i.e., results in generation

Table 1 Comparative summary of biosensors and assays for the determination of 17β-estradiol, reported in literature

Assay/biosensor platform	Mode of detection	Limit of detection (dynamic linear range)	References
Poly(β-cyclodextrin)/aptamer	Electrochemical aptasensor	0.7fM (1×10^{-13} – 1×10^{-9} M)	[27]
Poly(4,7-bis(5-(3,4-ethylenedioxythiophene)thiophen-2-yl)benzo-thiadiazole)/HRP	Electrochemical enzymatic biosensor	105 nM (0.1–200 μM)	[7]
ER-α antibody	Electrochemical immunosensor	– (8–8272 pM)	[2]
HRP coupled to a DNA aptamer	Photoluminescence (fluorescence) apatasensor	0.7 pM (3.6–367 pM)	[74]
High-performance liquid chromatography and spectrometry	(1) Optical (UV–Vis) (2) Chromatography	0.5 μM (1.8–44 μM) 0.04 μM (0.2–22 μM)	[75]
AuE/PANI:(3MPA-ZnSeQDs)/HRP	Electrochemical enzymatic, aerobic	0.2 μM (0.05–4 μM)	This work

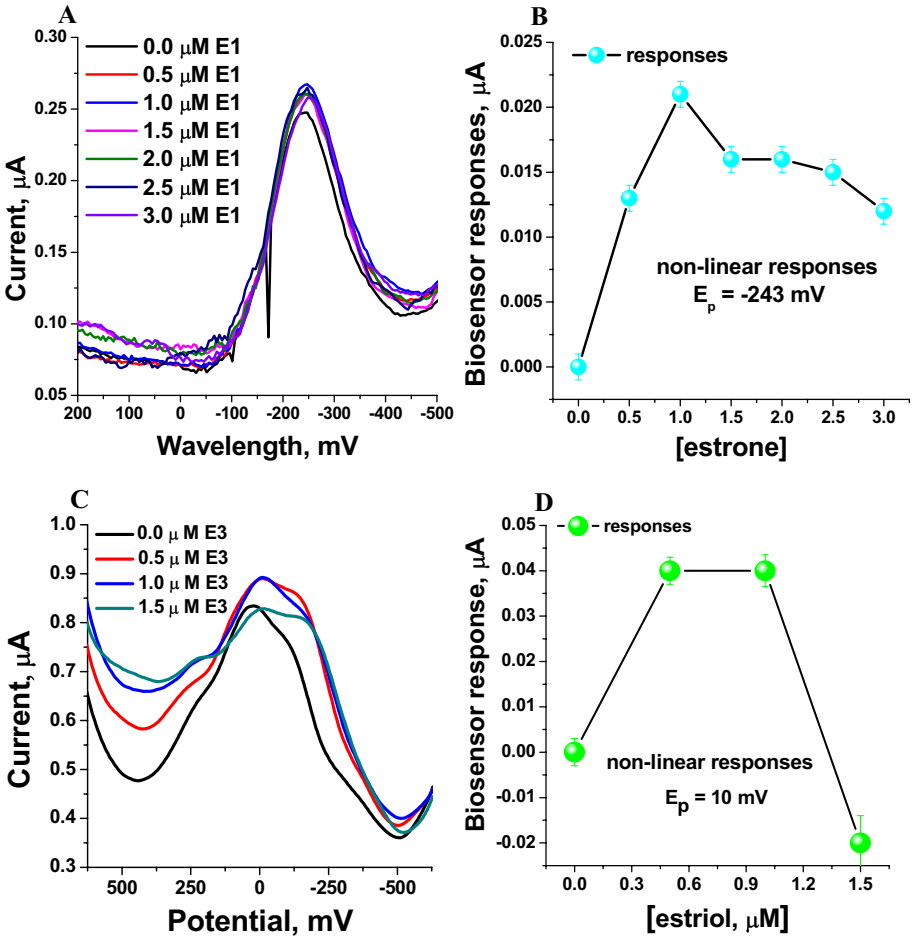

Fig. 7 **A**, **C**, **E** The AuE/PANI:3MPA-ZnSeQD/HRP biosensor responses to successive concentrations of estrone (E1), striol (E3), and 17α-ethinylestradiol (EE2). **B**, **D**, **F** The corresponding response curves. **G** Comparison of biosensor responses to various analytes; estrone, 17β-estradiol, estriol, and 17α-ethinylestradiol

of reactive oxygen species) such that many strategies have been developed to remove its residuals in treated water. The influence of low and high concentrations (i.e., 2 and 10 mM) of H_2O_2 on the electrochemical detection of 17β-estradiol was investigated using cyclic voltammetry. The electrochemical responses are shown in Fig. 8.

H_2O_2 evidently influenced the detection of 17β-estradiol, hence its removal is mandatory for analysis of real samples using the developed biosensor. This is obviously due to the high affinity of the HRP enzyme bio-receptor immobilized on the electrode interface to hydrogen peroxide [77]. Although this might be the case, it is also important to note that the electro-catalytic responses to different concentrations of hydrogen peroxide were facilitated at a distinct potential of − 340 mV, which was significantly higher than the potential at which the 17β-estradiol was detected. In a recent study, Fei fei Wang and co-workers utilized the granular activated carbon to sequentially quench the bromate ions and residual

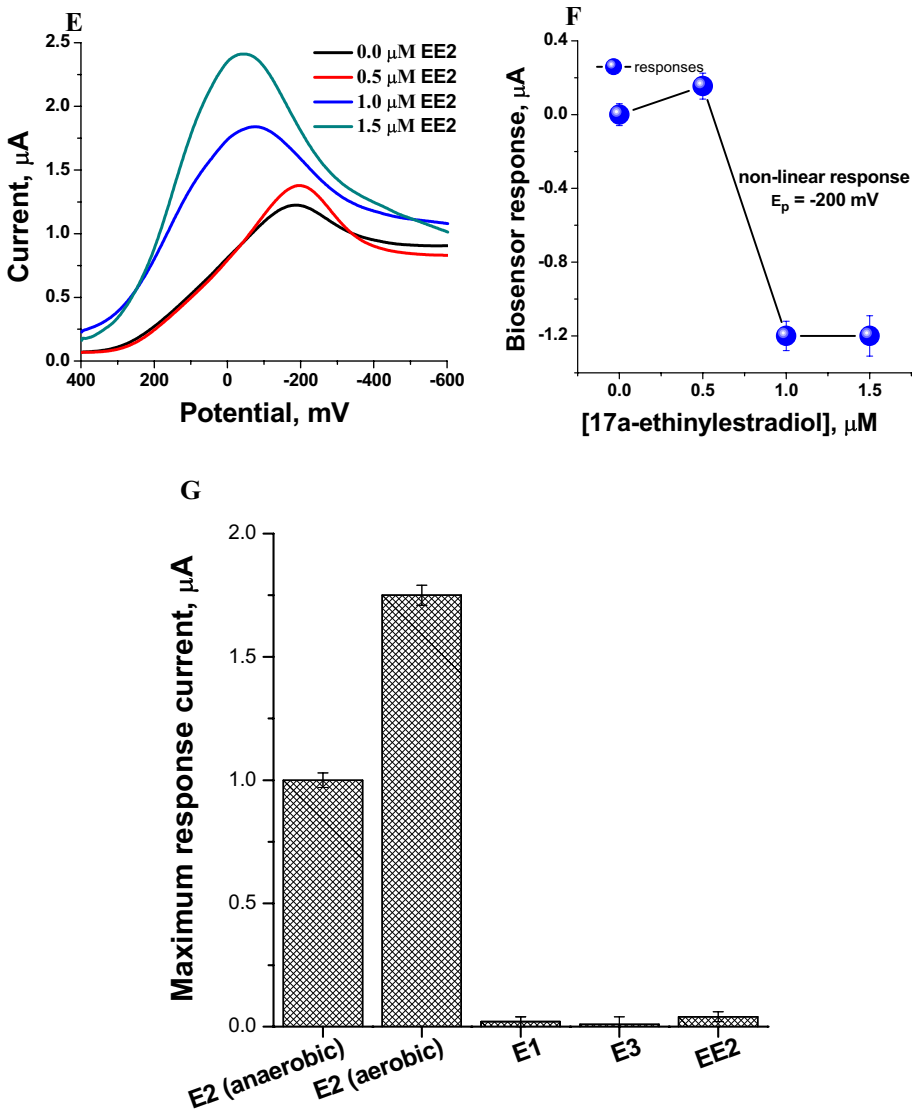

Fig. 7 (continued)

hydrogen peroxide [78]. Another strategy was proposed by Tingting Wu and co-workers where they employed sodium carbonate ions and heat to catalytically decompose H_2O_2 [79]. Due to high probability of the HRP enzyme mobilized on the biosensor electrode to catalyze H_2O_2, the biosensors has the high capacity to decompose or eliminate H_2O_2 and convert it into water by switching the redox onset potential prior, 17β-estradiol measurements. During real-field application of the proposed biosensor, the analysis could be preferable conducted in pre-treated water-water samples, such as tap water and other water bodies that do not contain trace concentrations of hydrogen peroxide. The reported biosensor

presents the simplest and straightforward alternative strategy to monitor and measure the concentrations of 17β-estradiol compared to lab-based traditional methods, such as chromatography, spectrometry, and ELISA, as most electrochemical sensors and biosensors could be easily configured and miniaturized into portable detection systems.

The Detection of 17β-Estradiol in Real Samples

In order to confirm the feasibility of the developed electrochemical nanobiosensor to quantify the 17β-estradiol, water samples were spiked with different concentrations of 17β-estradiol and analyzed using the biosensor. As depicted in Fig. 9, 17β-estradiol concentrations in tap water samples were capable of being detected by the developed biosensor, as there was a significant difference in the DPV responses for the un-spiked and spiked samples. The obtained recovery rates and relative standard deviation for each measured concentrations were determined and are summarized Table 2. The recovery rates from 101.35 to 133.3% were obtained. At low concentrations of 17β-estradiol in tap water, there was no deviation between the same concentration measurements ($n=2$). However, when the concentration of 17β-estradiol was increased to ≥ 3 µM, the relative standard deviation ($n=2$) significantly increased to 7%. Hence, the obtained data suggests that the developed biosensor was capable of being applied for real-field analysis of 17β-estradiol in water, and exhibited high efficiency to quantify 17β-estradiol, especially at low concentrations ≤ 2 µM. 17β-estradiol exhibit detrimental health impact on many species at even low accumulative concentrations.

The Re-usability and Stability of the Developed Biosensor

To investigate the potential of the developed biosensor films to be re-used, freshly prepared biosensor films were employed to measure six different concentrations of 17β-estradiol,

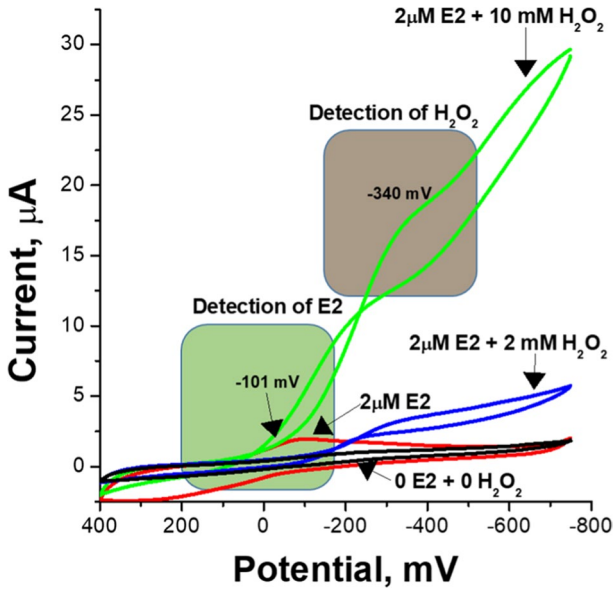

Fig. 8 The cyclic voltammetry responses of the AuE/PANI:3MPA-ZnSeQD/HRP biosensor in the presence of 2 µM 17β-estradiol (E2) + {2 and 10 mM H_2O_2} in 0.1 M phosphate buffer electrolyte solution of pH 7

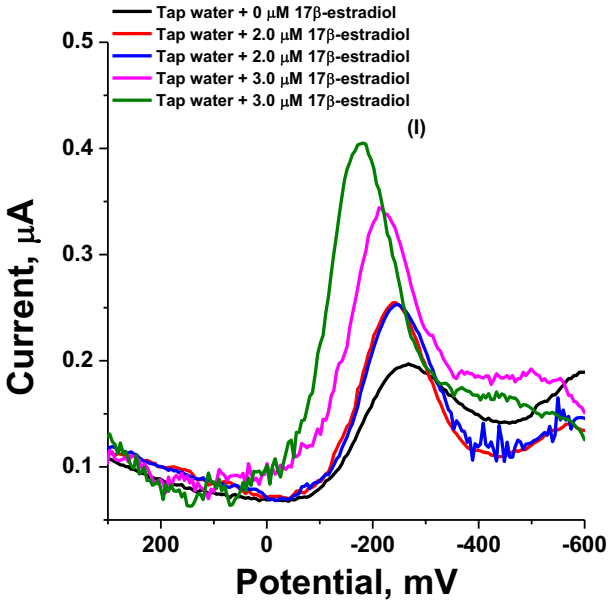

Fig. 9 DPV responses of the AuE/PANI:3MPA-ZnSeQD/HRP biosensor in tap water samples spiked with 0, 2, and 3 μM β-estradiol

Table 2 Real sample analysis of 17β-estradiol

Samples	Spiked (μM)	Current (μA)	Detected (μM)	Recovery (%)	RSD ($n=2$) (%)
Tap water	0	–	–	–	–
	2	0.25	2.027	101.35	0
		0.25	2.027	101.35	
	3.0	0.33	3.108	103.6	7
		0.40	4.0	133.3	

at consecutive number of measurements, denoted in Fig. 10 as measurements 1, 2, and 3. After each measurement, the biosensor surface was recovered through flashing the biosensor transducer with de-ionized water and phosphate buffer solution. This was done for the purpose of removing unwanted traces of materials that might have been loosely adhered on the surface in-between measurements. The AuE/PANI:3MPA-ZnSeQD/HRP biosensor catalytic current responses in Fig. 10 indicated that the number of times the biosensor was used for measurements and played a significant role in the catalytic current responses obtained. This evidently indicated loss of catalytic activity of the HRP enzyme mobilized on the bio-transducer surface. The percentage recovery obtained for the second set of measurements was significantly low. Relatively, for the third set of measurements, a percentage recovery of 27% was obtained. This is ascribed to the complete loss of catalytic activity sustained by the biosensor films. During E2 catalytic measurements with the biosensor, the products formed during the electro-catalytic reaction might have adsorbed on the biosensor surface thus inhibiting further enzyme activity. The drastic decrease of the catalytic activity could also be attributed to de-adsorption of the enzyme HRP from the biosensor surface during the soaking and recycling processes.

The AuE/PANI:3MPA-ZnSeQD/HRP Bio-sensor Electrode Mechanism

HRP enzyme has an α-helical 3D complex structure with hemi-active site [80–82] consisting of single polypeptide chain with 308 amino acid residues [54]. Almost all the catalytic reactions involving the HRP occur at the active site or relatively approximate to it. Although, HRP is known to catalyze the reductive splitting of H_2O_2 into H_2O molecules, this enzyme can intern bind, catalyze a series of phenolic compound, induce splitting of RO-OH bonds [54], and mediate hydroxylation of a range of compounds [52]. This is a very similar mechanism and approach adopted by cytochrome-P450 enzymes to bind to steroids, hence its choice for this particular application. The catalytic active site of HRP is illustrated in Fig. 11A, a representation abstracted from studies reported in literature [76, 83].

A proposed electrode mechanism was then derived and is illustrated in Fig. 11 (B). The mechanism is herein further interpreted by Eqs. (5) to (6). HRP catalyzes most of its reaction through its heme-center by transformation of its valance into different isoforms [83] also referred to as compound I and compound II [52]. According our the drawn-up mechanism, for alcohol oxidation by the monooxygenase peroxidase; the compound I preferable HRP-(Fe^{5+}) isoform catalytically reacts with the first alcohol (i.e., in this case 17β-estradiol) and transforms the HRP-Fe^{5+} catalytic center into a HRP-Fe^{4+} isoform (i.e., compound II); this is assumed to be a one electron reduction process. Further reduction of compound II results in re-generation of the resting state of the HRP enzyme (i.e., HRP-Fe^{3+}) [76]. The second addition of the alcohol displaces the water molecule that ready binds to the HRP-Fe^3-altered active site to attain stability. Simultaneously, the alcohol derivative is oxidized during this process.

$$\mathrm{HRP} - \mathrm{Fe}^{3+} + \mathrm{H_2O} + \mathrm{O_2} \rightarrow \mathrm{HRP} - \mathrm{Fe}^{5+}\left(\mathrm{H_2O}\right) + 2\mathrm{e}^{-}(2\mathrm{e} - \mathrm{redoxstep}) \tag{5}$$

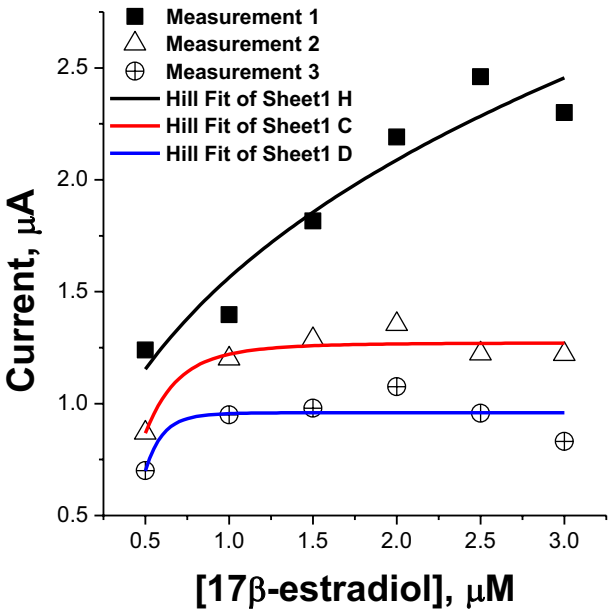

Fig. 10 The influence of single and multiple E2 measurements on the electrocatalytic performance of the AuE/PANI:3MPA-ZnSeQD/HRP biosensor electrode

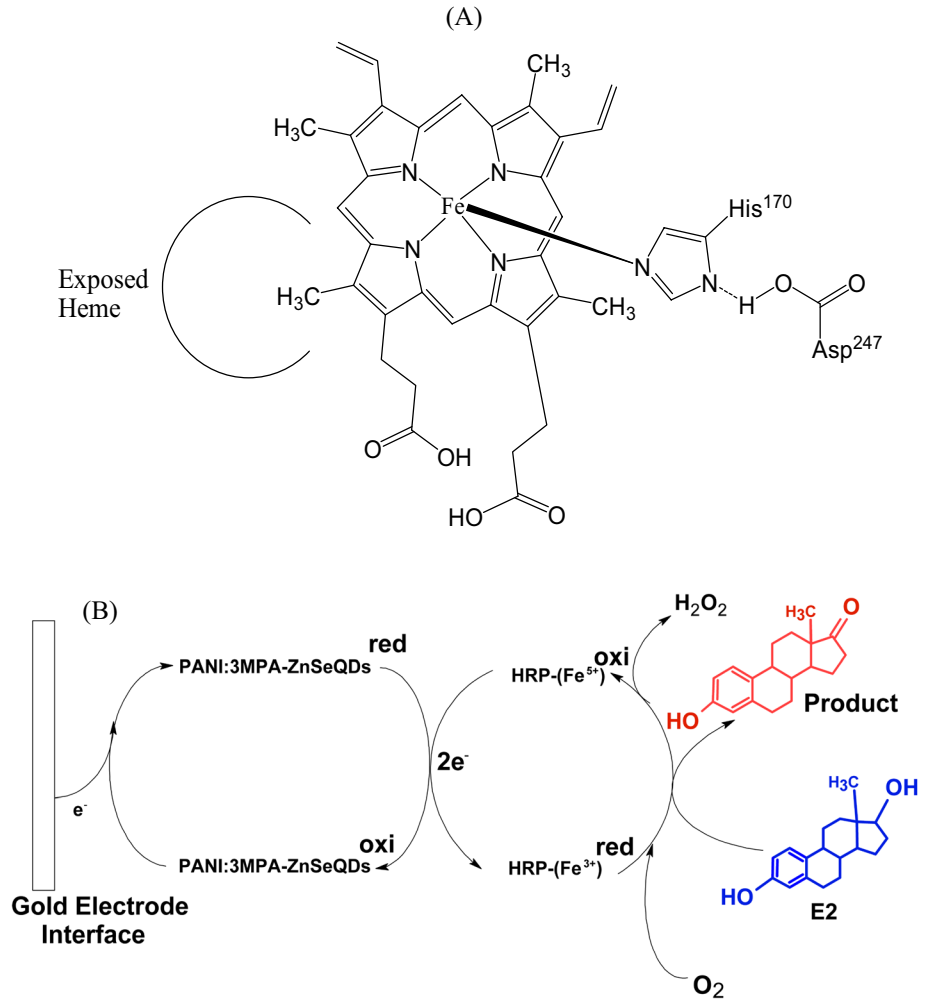

Fig. 11 **A** The chemical sstructure of the heme-active site of the horseradish peroxidase (HRP) enzyme and the **B** the proposed electron transfer mechanism occurring on the AuE/PANI:3MPA-ZnSeQD/HRP biotransducer interface

$$HRP - Fe^{5+} + e^{-} + RCH_2OH \rightarrow HRP - Fe^{4+} + RCH_2OH - (OH),\ Ep = -205mV(\text{hydroxylation of E2}) \quad (6)$$

The compound RCH_2OH in this case is assumed to be 17β-estradiol and RCH_2CO-(OH) is the oxidized product of 17β-estradiol.

Conclusion

Ultra-small 3-mercaptopropionic acid-capped ZnSe quantum dots of 5.3 ± 0.93 nm were successfully produced and captured onto the PANI nanofibers during electrochemical polymerization. The carboxylic acid functional groups from the 3-mercaptopropionic acid

capping ligand onto the surface of quantum dots facilitated the quantum dots to attach to the PANI. On the other hand, the conserved functionalities from both the PANI and 3MPA-ZnSe quantum dots also enhanced the surface susceptibility for attachment of the HRP bio-receptor onto the electrode surface. The attachment of the HRP enzyme was not only arbitrated by the chemical reactivity of the surface, but also further enhanced by available abundant active sites attributable to high surface area to volume ratio contributed by both the nano-sized PANI and small-sized 3MPA-ZnSe quantum dots. The AuE/PANI:3MPA-ZnSeQD/HRP biosensor constructed from the polyaniline and ZnSe quantum dots conjugated to HRP enzyme demonstrated excellent capacity to detect variable concentrations of 17β-estradiol under both aerobic and anaerobic environment conditions. The catalytic activities of the horseradish peroxidase enzyme immobilized on the electrode surface was slight distinct in the presence and absence of the oxygen molecules in the electrolyte solution. This was assigned to the transformation of the HRP isoform to an alternative redox state due to oxygen binding at the enzyme active catalytic site. This was also supported by a significant shift in the formal potential where the 17β-estradiol/biosensor interaction was observed upon introducing an influx of oxygen molecules. The biosensor also exhibited good specificity towards the determination of 17β-estradiol concentrations compared to structural similar compounds; a low detection limit and much more improved overall sensing parameters were obtained. Due to high reactivity of the HRP immobilized on the biosensor electrode surface to H_2O_2, the hydrogen peroxide induced redox activity, however at high negative redox potentials of –340 mV. Hence in the presence of H_2O_2, the AuE/PANI:3MPA-ZnSeQD/HRP biosensor, specifically the HRP attached on the biosensor induced catalysis at a significantly different potential than observed for 17β-estradiol analyte. This is attributable to the pre-activation of the HRP active center by the hydrogen peroxide molecules; this has been proven to transform the Fe(V) valance state of the HRP enzyme into a different oxidation state or isoform. The portable miniaturized electrochemical biosensors are programmed at a single potential value, where the electrochemical catalysis of the analyte of interest is observed. Hence, H_2O_2 might not interfere significantly during the real application of the biosensor. Nonetheless, many strategies to eliminate H_2O_2 are integral part of wastewater reclamation procedures; hence, H_2O_2 is not much of a major interfering species. In conclusion, the biosensor was capable of detecting 17β-estradiol concentrations in spiked tap water samples with good recoveries.

Supplementary Information The online version contains supplementary material available at https://doi.org/10.1007/s12010-022-04277-w.

Author Contribution Abongile Jijana–conceptualization, assimilation of the presented data, and preparation of the manuscript.

Funding The research project was fully funded by the Department of science technology (DST) of South Africa through the National Research Foundation (NRF) funding mechanism.

Data Availability All manuscript data will be made available from the author upon reasonable request with permission granted by parties: Mintek and University of the Western Cape.

Declarations

Ethics Approval No ethical clearance was required during for his research, as the study does not use any human or animal derived material or samples.

Consent to Participate All authors of this manuscript granted consent to partake in the research undertaken.

Consent to Publish All authors of the manuscript herein listed, gave consent to publish the presented data including all figures and supplementary material.

Competing Interest The author declares no competing interests.

References

1. Bai, J., Gao, Z., Wang, W., Peng, Y., Wu, J., Zhang, M., … Cao, G. (2021). Ultrasensitive detection of 17β-estradiol (e2) based on multistep isothermal amplification. *Analytical Chemistry*, *93*(10), 4488–4496.https://doi.org/10.1021/acs.analchem.0c04681
2. Dai, Y., & Liu, C. C. (2017). Detection of 17 β -Estradiol in environmental samples and for health care using a single-use , cost-effective biosensor based on differential pulse voltammetry (DPV). *Biosensors*, *7*(15). https://doi.org/10.3390/bios7020015
3. Saaristo, M., Craft, J. A., Lehtonen, K. K., & Lindström, K. (2010). An endocrine disrupting chemical changes courtship and parental care in the sand goby. *Aquatic Toxicology, 97*(4), 285–292. https://doi.org/10.1016/j.aquatox.2009.12.015
4. Jensen, E. V., Jacobson, H. I., Walf, A. A., & Frye, C. A. (2010). Estrogen action: A historic perspective on the implications of considering alternative approaches. *Physiology and Behavior, 99*(2), 151–162. https://doi.org/10.1016/j.physbeh.2009.08.013
5. Emna, D., Yahia, M. N. D., Farcy, E., Pringault, O., & Bonnet, D. (2022). Acute and chronic toxicity assessments of 17β-estradiol (E2) and 17a-ethinylestradiol on the calanoid.pdf. *Science of the Total Environment Journal*. https://doi.org/10.1016/j.scitotenv.2021.150845
6. Shappell, N. W., Hyndman, K. M., Bartell, S. E., & Schoenfuss, H. L. (2010). Comparative biological effects and potency of 17α- and 17β-estradiol in fathead minnows. *Aquatic Toxicology, 100*(1), 1–8. https://doi.org/10.1016/j.aquatox.2010.07.005
7. Spychalska, K., Zając, D., & Cabaj, J. (2020). Electrochemical biosensor for detection of 17β-estradiol using semi-conducting polymer and horseradish peroxidase. *RSC Advances, 10*(15), 9079–9087. https://doi.org/10.1039/c9ra09902f
8. Schilirò, T., Pignata, C., Rovere, R., Fea, E., & Gilli, G. (2009). The endocrine disrupting activity of surface waters and of wastewater treatment plant effluents in relation to chlorination. *Chemosphere, 75*(3), 335–340. https://doi.org/10.1016/j.chemosphere.2008.12.028
9. Chang, H. S., Choo, K. H., Lee, B., & Choi, S. J. (2009). The methods of identification, analysis, and removal of endocrine disrupting compounds (EDCs) in water. *Journal of Hazardous Materials, 172*(1), 1–12. https://doi.org/10.1016/j.jhazmat.2009.06.135
10. Alda, M. J. L., & Barcelo, D. (2000). Determination of steroid sex hormones and related synthetic compounds considered as endocrine disrupters in water by liquid chromatography – diode array detection – mass spectrometry. *Journal of Chromatography A, 892*, 391–406.
11. Guo, Y., Han, Z., Min, H., Chen, Z., Sun, T., Wang, L., … Cheng, P. (2022). Bilanthanide metal–organic frameworks for instant detection of 17β-estradiol, a vital physiological index. *Small Structures*, *3*(5), 2100113.https://doi.org/10.1002/sstr.202100113
12. Wang, A., Ding, Y., Li, L., Duan, D., Mei, Q., Zhuang, Q., … He, X. (2019). A novel electrochemical enzyme biosensor for detection of 17β-estradiol by mediated electron-transfer system. *Talanta*, *192*(September 2018), 478–485. https://doi.org/10.1016/j.talanta.2018.09.018
13. Sesay, A. M., & Cullen, D. C. (2001). Detection of hormone mimics in water using a miniturised SPR sensor. *Enviromental Monitoring and Assessment, 70*, 83–92.
14. Campbell, C. G., Borglin, S. E., Green, F. B., Grayson, A., Wozei, E., & Stringfellow, W. T. (2006). Biologically directed environmental monitoring, fate, and transport of estrogenic endocrine disrupting compounds in water : A review. *Chemosphere, 65*, 1265–1280. https://doi.org/10.1016/j.chemosphere.2006.08.003
15. Szabó, R., Hoffmann, A., Börzsei, D., Kupai, K., Veszelka, M., Berkó, A. M., … Varga, C. (2021). Hormone replacement therapy and aging: A Potential therapeutic approach for age-related oxidative stress and cardiac remodeling. *Oxidative Medicine and Cellular Longevity*, *2021*.https://doi.org/10.1155/2021/8364297
16. McMenamin, Ú., Hicks, B., Hughes, C., Murchie, P., Hippisley-Cox, J., Ranger, T., … Cardwell, C. (2021). Hormone replacement therapy in women with cancer and risk of cancer-specific mortality and

cardiovascular disease: a protocol for a cohort study from Scotland and Wales. *BMC Cancer*, *21*(1), 4–9.https://doi.org/10.1186/s12885-021-08065-3
17. Preedy, J. R. K., & Aitken, E. H. (1961). The Determination of estrone, estradiol-17β, and Estriol in urine and plasma with column partition chromatography. *Journal of Biological Chemistry, 236*(5), 1300–1311. https://doi.org/10.1016/S0021-9258(18)64169-9
18. Nili-Ahmadabadi, A., Rezaei, F., Heshmati, A., Ranjbar, A., & Larki-Harchegani, A. (2021). Steroid Hormone exposure as a potential hazard in milk consumers: A significant health challenge in Iran. *Journal of Food Quality*, *2021*.https://doi.org/10.1155/2021/5595555
19. Zheng, W., Yates, S. R., & Bradford, S. A. (2008). Analysis of steroid hormones in a typical dairy waste disposal system. *Environmental Science and Technology, 42*(2), 530–535. https://doi.org/10.1021/es071896b
20. Mehta, J., Kling, J. M., & Manson, J. A. E. (2021). Risks, Benefits, and treatment modalities of menopausal hormone therapy: Current concepts. *Frontiers in Endocrinology, 12*(March), 1–14. https://doi.org/10.3389/fendo.2021.564781
21. Maurício, R., Dias, R., Ribeiro, V., Fernandes, S., Vicente, A. C., Pinto, M. I., … Mano, A. P. (2018). 17α-Ethinylestradiol and 17β-estradiol removal from a secondary urban wastewater using an RBC treatment system. *Environmental Monitoring and Assessment*.https://doi.org/10.1007/s10661-018-6701-8
22. Esmaeeli, F., Gorbanian, S. A., & Moazezi, N. (2017). Removal of estradiol valerate and progesterone using powdered and granular activated carbon from aqueous solutions. *International Journal of Environmental Research, 11*(5–6), 695–705. https://doi.org/10.1007/s41742-017-0060-0
23. Prokić, D., Vukčević, M., Mitrović, A., Maletić, M., Kalijadis, A., Janković-Častvan, I., & Đurkić, T. (2021). Adsorption of estrone, 17β-estradiol, and 17α-ethinylestradiol from water onto modified multi-walled carbon nanotubes, carbon cryogel, and carbonized hydrothermal carbon. *Environmental Science and Pollution Research*. https://doi.org/10.1007/s11356-021-15970-4
24. Nazari, E., & Suja, F. (2016). Effects of 17β-estradiol (E2) on aqueous organisms and its treatment problem: A review. *Reviews on Environmental Health, 31*(4), 465–491. https://doi.org/10.1515/reveh-2016-0040
25. Wee, S. Y., Aris, A. Z., Yusoff, F. M., & Praveena, S. M. (2020). Occurrence of multiclass endocrine disrupting compounds in a drinking water supply system and associated risks. *Scientific Reports, 10*(1), 1–12. https://doi.org/10.1038/s41598-020-74061-5
26. Domènech, A., Pich, S., Arís, A., Plasencia, C., Bach, A., & Serrano, A. (2011). Heat identification by 17β-estradiol and progesterone quantification in individual raw milk samples by enzyme immunoassay. *Electronic Journal of Biotechnology*. https://doi.org/10.2225/vol14-issue4-fulltext-6
27. Chang, Z., Zhu, B., Liu, J. J., Zhu, X., Xu, M., & Travas-Sejdic, J. (2021). Electrochemical aptasensor for 17β-estradiol using disposable laser scribed graphene electrodes. *Biosensors and Bioelectronics*. https://doi.org/10.1016/j.bios.2021.113247
28. Rozi, N., Hanifah, S. A., Zaid, M. H. M., Abd Karim, N. H., & Ikeda, M. (2021). Feasible study on poly(pyrrole-co-pyrrole-3-carboxylic acid)-modified electrode for detection of 17β-estradiol. *Chemical Papers, 75*(7), 3493–3503. https://doi.org/10.1007/s11696-021-01597-9
29. Sharma, V., & Mehata, M. S. (2021). Synthesis of photoactivated highly fluorescent Mn2+-doped ZnSe quantum dots as effective lead sensor in drinking water. *Materials Research Bulletin*, *134*(October 2020), 1–8. https://doi.org/10.1016/j.materresbull.2020.111121
30. Park, J. Y., Jeon, E. J., Choa, Y. H., & Kim, B. S. (2019). Optical and structural properties of ZnSe quantum dot with europium. *Journal of Luminescence*, *208*(June 2018), 145–149. https://doi.org/10.1016/j.jlumin.2018.12.018
31. Sharma, K., Raizada, P., Hasija, V., Singh, P., & Bajpai, A. (2021). ZnS-based quantum dots as photocatalysts for water purification Journal of Water Process Engineering ZnS-based quantum dots as photocatalysts for water purification. *Journal of Water Process Engineering*, *43*(July), 102217. Retrieved from https://doi.org/10.1016/j.jwpe.2021.102217
32. Stavrou, J. Y. H. E.-V. N. (2018). Biomolecule-conjugated quantum dot nanosensors as probes for cellular dynamic events in living cells (p. Ch. 7). Rijeka: IntechOpen. https://doi.org/10.5772/intechopen.72858
33. Suo, B., Su, X., Wu, J., Chen, D., Wang, A., & Guo, Z. (2010). Poly (vinyl alcohol) thin film filled with CdSe – ZnS quantum dots : Fabrication, characterization and optical properties. *Materials Chemistry and Physics, 119*, 237–242. https://doi.org/10.1016/j.matchemphys.2009.08.054
34. Wood, V., Chen, J., Panzer, M. J., Bradley, M. S., Halpert, J. E., Bawendi, M. G., & Bulović, V. (2008). Inkjet-printed quantum dot and polymer composites for AC-driven electroluminescent devices. *Advanced Materials, 115*, 8715.

35. Chen, H., Huang, H., & Chen, C. (2004). Quantum Dots / Conductive Polymer Nanocomposite. *NSTI-Nanotech, 3*, 34–36.
36. Fogg, D. E., Radzilowski, L. H., Blanski, R., Schrock, R. R., & Thomas, E. L. (1997). Fabrication of quantum dot/polymer composites phosphine-functionalized block copolymers as passivating hosts for cadmium selenide nanoclusters. *Macromolecules, 30*, 417–426.
37. Rafeeq, S. N., & Khalaf, W. Z. (2015). Preparation, characterization and electrical conductivity of doped polyaniline with (HCL and P - TSA). *Eng & Tech.Journal*, *33*(7).
38. Neelgund, G. M., & Oki, A. (2012). A facile method for synthesis of polyaniline nanospheres and effect of doping on their electrical conductivity. *Polymer International, 60*(9), 1291–1295. https://doi.org/10.1002/pi.3068.A
39. Wang, H., Lin, J., & Xiang, Z. (2016). Advanced materials and devices polyaniline (PANi) based electrode materials for energy storage and conversion. *Journal of Science: Advanced Materials and Devices, 1*(3), 225–255. https://doi.org/10.1016/j.jsamd.2016.08.001
40. Srinivas, C. H., Srinivasu, D., Kavitha, B., Narsimlu, N., & Kumar, K. S. (2012). Synthesis and characterization of nano size conducting polyaniline. *Journal of Applied Physics, 1*(5), 12–15.
41. Deshpande, N., Chakane, S., & Borude, R. R. (2016). Synthesis and characterization of polyaniline, using different dopant, for sensing application of pollutant gases. *Journal of Atomic, Molecular, Condensate & Nano Physics, 3*(1), 27–33.
42. Alice, M., Mazzeu, C., Faria, L. K., Cardoso, A. D. M., Gama, M., Baldan, M. R., & Gonçalves, E. S. (2017). Structural and morphological characteristics of polyaniline synthesized in pilot scale. *Journal of Aerospace Technology and Management, 9*, 39–47. https://doi.org/10.5028/jatm.v9i1.726
43. Bhadra, S., Khastgir, D., Singha, N. K., & Hee, J. (2009). Progress in polymer science progress in preparation, processing and applications of polyaniline. *Progress i Polymer Science, 34*, 783–810. https://doi.org/10.1016/j.progpolymsci.2009.04.003
44. Zhang, G., Li, X., Jia, H., Pang, X., Yang, H., Wang, Y., & Ding, K. (2012). Preparation and characterization of polyaniline (PANI) doped- Li3V2(PO4)3. *International Journal of Electrochemical Science, 7*, 830–843.
45. Krainer, F. W., & Glieder, A. (2015). An updated view on horseradish peroxidases: Recombinant production and biotechnological applications. *Applied Microbiology and Biotechnology, 99*(4), 1611–1625. https://doi.org/10.1007/s00253-014-6346-7
46. De Visser, S. P., Shaik, S., Sharma, P. K., Kumar, D., & Thiel, W. (2003). Active species of horseradish peroxidase (HRP) and cytochrome p450: Two electronic chameleons. *Journal of the American Chemical Society, 125*(51), 15779–15788. https://doi.org/10.1021/ja0380906
47. Sevrioukova, I. F., & Poulosa, T. L. (2013). Understanding the mechanism of cytochrome p450:Recent advances and remaining problemS. *Dalton Transactions, 42*(9), 3116–3126. https://doi.org/10.1039/c2dt31833d.UNDERSTANDING
48. Stavropoulou, E., Pircalabioru, G. G., & Bezirtzoglou, E. (2018). The role of cytochromes P450 in infection. *Frontiers in Immunology*, *9*(JAN), 1–7. https://doi.org/10.3389/fimmu.2018.00089
49. Ahirwal, G. K., & Mitra, C. K. (2009). Direct electrochemistry of horseradish peroxidase-gold nanoparticles conjugate. *Sensors (Basel, Switzerland), 9*(2), 881–894. https://doi.org/10.3390/s90200881
50. Vlasova, I. I. (2018). Peroxidase activity of human hemoproteins: Keeping the fire under control. *Molecules, 23*(10), 1–27. https://doi.org/10.3390/molecules23102561
51. Esteves, F., Rueff, J., & Kranendonk, M. (2021). The central role of cytochrome P450 in Xenobiotic metabolism—a brief review on a fascinating enzyme family. *Journal of Xenobiotics, 11*(3), 94–114. https://doi.org/10.3390/jox11030007
52. de Oliveira, F. K., Santos, L. O., & Buffon, J. G. (2021). Mechanism of action, sources, and application of peroxidases. *Food Research International*, *143*(October 2020). https://doi.org/10.1016/j.foodres.2021.110266
53. Xu, R., Chi, C., Li, F., & Zhang, B. (2013). Immobilization of horseradish peroxidase on electrospun microfibrous membranes for biodegradation and adsorption of bisphenol A. *Bioresource Technology, 149*, 111–116. https://doi.org/10.1016/j.biortech.2013.09.030
54. Nunavath, H., Banoth, C., Talluri, V. R., & Bhukya, B. (2016). An analysis of horseradish peroxidase enzyme for effluent treatment. *Bioinformation, 12*(06), 318–323. https://doi.org/10.6026/97320630012318
55. Zuccarello, L., Barbosa, C., Todorovic, S., & Silveira, C. M. (2021). Electrocatalysis by heme enzymes—applications in biosensing. *Catalysts, 11*(2), 1–44. https://doi.org/10.3390/catal11020218

56. Guo, Y., & Guadalupe, A. R. (1997). Direct electrochemistry of horseradish peroxidase adsorbed on glassy carbon electrode from organic solutions. *Chemical Communications, 15*, 1437–1438. https://doi.org/10.1039/A703254D
57. Vineh, M. B., Saboury, A. A., Poostchi, A. A., & Ghasemi, A. (2020). Biodegradation of phenol and dyes with horseradish peroxidase covalently immobilized on functionalized RGO-SiO2 nanocomposite. *International Journal of Biological Macromolecules, 164*, 4403–4414. https://doi.org/10.1016/j.ijbiomac.2020.09.045
58. Naveen, M. H., Gurudatt, N. G., & Shim, Y. B. (2017). Applications of conducting polymer composites to electrochemical sensors: A review. *Applied Materials Today, 9*, 419–433. https://doi.org/10.1016/j.apmt.2017.09.001
59. Mohamad Ahad, I. Z., Wadi Harun, S., Gan, S. N., & Phang, S. W. (2018). Polyaniline (PAni) optical sensor in chloroform detection. *Sensors and Actuators, B: Chemical, 261*, 97–105. https://doi.org/10.1016/j.snb.2018.01.082
60. Hiragond, C. B., Khanna, P. K., & More, P. V. (2018). Probing the real-time photocatalytic activity of CdS QDs sensitized conducting polymers: Featured PTh, PPy and PANI. *Vacuum, 155*, 159–168. https://doi.org/10.1016/j.vacuum.2018.06.009
61. Baruah, J. M., Kalita, S., & Narayan, J. (2019). Green chemistry synthesis of biocompatible ZnS quantum dots (QDs): Their application as potential thin films and antibacterial agent. *International Nano Letters, 9*(2), 149–159. https://doi.org/10.1007/s40089-019-0270-x
62. Memon, U. B., Chatterjee, U., Gandhi, M. N., Tiwari, S., & Duttagupta, S. P. (2014). Synthesis of ZnSe quantum dots with stoichiometric ratio difference and study of its optoelectronic property. *Procedia Materials Science, 5*, 1027–1033. https://doi.org/10.1016/j.mspro.2014.07.393
63. Shen, F., Que, W., Liao, Y., & Yin, X. (2011). Photocatalytic activity of TiO2 nanoparticles sensitized by CuInS 2 quantum dots. *Industrial & Engineering Chemistry Research, 50*(15), 9131–9137. https://doi.org/10.1021/ie2007467
64. Senthilkumar, K., Kalaivani, T., Kanagesan, S., Balasubramanian, V., & Balakrishnan, J. (2013). Wurtzite ZnSe quantum dots: Synthesis, characterization and PL properties. *Journal of Materials Science: Materials in Electronics, 24*(2), 692–696. https://doi.org/10.1007/s10854-012-0796-4
65. Yang, Z., & Chang, H.-T. (2010). CdHgTe and CdTe quantum dot solar cells displaying an energy conversion efficiency exceeding 2%. *Solar Energy Materials and Solar Cells, 94*(12), 2046–2051. https://doi.org/10.1016/j.solmat.2010.06.013
66. Korlann, S. D., Riley, A. E., Kirsch, B. L., Mun, B. S., & Tolbert, S. H. (2005). Chemical tuning of the electronic properties in a periodic surfactant-templated nanostructured semiconductor. *Journal of the American Chemical Society, 127*(36), 12516–12527. https://doi.org/10.1021/ja045446k
67. Ma, Y., Fan, G.-C., Cui, M., Gu, S., Liu, Q., & Luo, X. (2019). Novel cathodic photoelectrochemical immnuosensor with high sensitivity based on 3D AuNPs/ZnO/Cu2O heterojunction nanowires. *Electrochimica Acta, 318*, 100–107. https://doi.org/10.1016/j.electacta.2019.05.160
68. Ndangili, P. M., Arotiba, O. A., Baker, P. G. L., & Iwuoha, E. I. (2010). A potential masking approach in the detection of dopamine on 3-mercaptopropionic acid capped ZnSe quantum dots modified gold electrode in the presence of interferences. *Journal of Electroanalytical Chemistry, 643*(1–2), 77–81. https://doi.org/10.1016/j.jelechem.2010.03.006
69. Karimi, A., Mahdizadeh, F., Salari, D., Vahabzadeh, F., & Khataee, A. (2012). Enzymatic scavenging of oxygen dissolved in water: Application of response surface methodology in optimization of conditionS In. *Chemical Industry and Chemical Engineering Quarterly, 18*(3), 431–439. https://doi.org/10.2298/CICEQ110823020K
70. Silverstein, T. P., & Goodney, D. E. (2010). Enzyme-linked biosensors: Michaelis-Menten kinetics need not apply. *Journal of Chemical Education, 87*(9), 905–907. https://doi.org/10.1021/ed100381r
71. Al-ahmed, A., Ndangili, P. M., Jahed, N., Baker, P. G. L., & Iwuoha, E. I. (2009). Polyester Sulphonic acid interstitial nanocomposite platform for peroxide biosensor. *Sensors, 9*, 9965–9976. https://doi.org/10.3390/s91209965
72. Fersht, A. (1985). *Enzyme Structure and Mechanism, Second Edition*. W.H Freman and Company.
73. Walsh, C. (1979). *Enzyme reaction mechanism*. W.H Freman and Company.
74. Yang, H., & Xu, D. (2022). Highly-sensitive and simple fluorescent aptasensor for 17 b-estradiol detection coupled with HCR-HRP structure. *Talanta*, *240*(November 2021). https://doi.org/10.1016/j.talanta.2021.123094
75. Yilmaz, B., & Kadioglu, Y. (2017). Determination of 17 β-estradiol in pharmaceutical preparation by UV spectrophotometry and high performance liquid chromatography methods. *Arabian Journal of Chemistry, 10*, S1422–S1428. https://doi.org/10.1016/j.arabjc.2013.04.018
76. Veitch, N. C. (2004). Horseradish peroxidase: A modern view of a classic enzyme. *Phytochemistry, 65*(3), 249–259. https://doi.org/10.1016/j.phytochem.2003.10.022

77. Pandey, V. P., Awasthi, M., Singh, S., Tiwari, S., & Dwivedi, U. N. (2017). A Comprehensive review on function and application of plant peroxidases. *Biochemistry & Analytical Biochemistry, 06*(01), 1–16. https://doi.org/10.4172/2161-1009.1000308
78. Wang, F., Zhang, L., Wei, L., & Van Der Hoek, J. P. (2021). Removal of hydrogen peroxide residuals and by-product bromate from advanced oxidation processes by granular activated carbon. *Water*, *13*(18). https://doi.org/10.3390/w13182460
79. Wu, T., & Englehardt, J. D. (2012). A New method for removal of hydrogen Peroxide Interference in the Analysis of Chemical Oxygen Demand. *Environmental Science & Technology, 46*(4), 2291–2298. https://doi.org/10.1021/es204250k
80. Lee, Y.-M., Kwon, O.-Y., Yoon, Y.-J., & Ryu, K. (2006). Immobilization of horseradish peroxidase on multi-wall carbon nanotubes and its electrochemical properties. *Biotechnology Letters, 28*(1), 39–43. https://doi.org/10.1007/s10529-005-9685-8
81. Veitch, N. (2004). Veitch, N. C. Horseradish peroxidase: A modern view of a classic enzyme. Phytochemistry 65, 249–259. *Phytochemistry, 65*, 249–259. https://doi.org/10.1016/j.phytochem.2003.10.022
82. Lee, A.-C., Liu, G., Heng, C.-K., Tan, S.-N., Lim, T.-M., & Lin, Y. (2008). Sensitive electrochemical detection of horseradish peroxidase at disposable screen-printed carbon electrode. *Electroanalysis, 20*(18), 2040. https://doi.org/10.1002/elan.200804287
83. Khanmohammadi, M., Dastjerdi, M. B., Ai, A., Ahmadi, A., Godarzi, A., Rahimi, A., & Ai, J. (2018). Horseradish peroxidase-catalyzed hydrogelation for biomedical applications. *Biomaterials Science, 6*(6), 1286–1298. https://doi.org/10.1039/c8bm00056e

Authors and Affiliations

Abongile Nwabisa Jijana[1,2]

[1] Nanotechnology Innovation Centre, Advanced Material Division, Mintek, 200 Malibongwe Drive, Private Bag X 3015, Johannesburg, Gauteng, South Africa

[2] SensorLab, Department of Chemistry, University of the Western Cape, Robert Sobukwe Rd, Bellvile, P.O. Box X75, Cape Town 7535, South Africa